PHYSICAL PROPERTIES OF SEDIMENTS IN THE NANKAI TROUGH ACCRETIONARY PRISM

by

Nicole Wiersgalla Hoffman

Submitted in Partial Fulfillment

of the Requirements for the Degree of

Master of Science in Geophysics

New Mexico Institute of Mining and Technology

Socorro, New Mexico

May, 2004

ABSTRACT

The Nankai Trough accretionary prism of southwest Japan is an excellent setting to characterize the physical properties of marine sediments as they are initially deformed, accreted and underthrust. The formation of the basal décollement in an accretionary prism is a result of a zone of weakness due to high pore pressure located in the incoming sediment section. In order to quantify and document regional variations in porosity and pore pressure in the underthrust section, a transform between seismic velocity and porosity is necessary. I present a formulation to convert seismic velocity to porosity based on a previously developed empirical relationship that incorporates a critical porosity transition. Shipboard laboratory measurements of velocity and porosity from ODP Legs 131, 190 and 196 along the Muroto transect are used to constrain the parameters for the velocity-porosity transform. Corrections to account for unloading from in-situ conditions have been applied to the core data. A critical porosity transition appears to be crossed in the sediments between the protothrust and frontal thrust zones of the prism at a fractional porosity of $\sim$0.30.

I present evidence for the effects of silica diagenesis on physical properties at the reference site for the Nankai Trough. Anomalous porosity and

velocity values in the Shikoku Basin facies suggest that processes factors in addition to normal burial consolidation are affecting the physical properties of the sediments. The location of the boundary between the upper and lower Shikoku basin facies is influenced in part by the opal-A to opal-CT transition. I present an analysis suggesting that an anomalously high porosity zone from 100-344 mbsf is held open by silica cementation which is subsequently destroyed at the opal-A to opal-CT transition at $\sim$ 344 mbsf.

ACKNOWLEDGMENTS

This research was funded with a research assistantship provided by JOI-USSSP. Special thanks to Ian M. Hoffman for his assistance with the non-linear least-squares parameter fitting and his wonderful support.

This thesis was typeset with LaTeX[1] by the author.

[1] LaTeX document preparation system was developed by Leslie Lamport as a special version of Donald Knuth's TeX program for computer typesetting. TeX is a trademark of the American Mathematical Society. The LaTeX macro package for the New Mexico Institute of Mining and Technology thesis format was adapted from Gerald Arnold's modification of the LaTeX macro package for The University of Texas at Austin by Khe-Sing The.

TABLE OF CONTENTS

LIST OF TABLES

LIST OF FIGURES

CHAPTER 1

INTRODUCTION

The accumulation of sediment at convergent margins is an important component of the initial mountain-building process. Accretionary processes have been regarded as a dominant mechanism for the crustal evolution of orogenic belts in both North America and Asia (Taira et al., 1989). In accretionary prisms sediment deformation and physical property changes occur very differently from ordinary sedimentary basins (Shipboard Scientific Party, 1991). Because of their relative structural simplicity, accretionary prisms provide an excellent setting to study the interaction between deformation and hydrologic processes at varying scales. In addition, the evolution of the sediment properties as they are incorporated into the prism can be compared to laboratory results to provide constraints on the mechanical behavior and stress paths within the prism (Karig and Morgan, 1994).

An accretionary prism is commonly composed of a series of imbricate thrust sheets of offscraped sediments which accumulate in the trench and ocean basin of the subducting plate (Karig and Morgan, 1994). An important component of the prism is the low-angle thrust fault, or the basal décollement, which separates the prism sediments from the subducting plate. The décollement plays an important role in the hydrologic processes in accretionary prisms and has a major impact on structural development in the accretionary prism

(Moore, 1989). This boundary also marks a change in the orientation of the stresses and a zone of stress decoupling (Moore, 1989; Morgan and Karig, 1995). Sediments located above the décollement are characterized by deformation features that generally indicate horizontal shortening (e.g. Lallemant et al., 1993). In contrast, the sediments located beneath the décollement, or the underthrust sediments, have few deformation structures and exhibit properties that are consistent with uniaxial consolidation (Morgan and Karig, 1995). Underthrust sediments also play an important role in the hydrology of the prism as they remain relatively unconsolidated compared to the overlying prism sediments (e.g. Le Pichon et al., 1993).

The décollement zone is thought to be preferentially developed at the top of or within a zone of high pore pressure present in the incoming sediments (e.g. Davis et al., 1983; Moore, 1989). In addition to controlling the location of the décollement zone, pore pressure in the underthrust sediments also likely controls the strength of the décollement zone (e.g. Byrne and Fisher, 1990). A weak décollement zone will result in an overlying prism with a small taper angle; a strong décollement will result in a high taper angle (Byrne and Fisher, 1990; Davis et al., 1983). Quantification of pore fluid pressure and porosity is therefore an important objective to advance understanding of décollement zone processes.

The Nankai Trough accretionary prism of southwest Japan (Figs. 1.1 and 1.2) is a well studied prism that provides an excellent setting to study the properties of the underthrust sediments through initial deformation and décollement formation (Moore et al., 2001). The décollement forms in relatively

homogeneous hemipelagic silty clay (Taira, Hill and Firth, et al., 1991) and represents an opportunity to study the contrast in physical properties and structural features across this boundary (Morgan and Karig, 1995). The entire thickness of the underthrust section along the Muroto transect off Shikoku Island (Fig. 1.2) has been sampled at several locations through coring and logging.

A potential source of information on porosity and pore pressure in the underthrust sediments is available from marine seismic reflection data. A transform between compressional wave velocity and porosity can be used to convert high-resolution seismic velocity to porosity. Numerous studies have been conducted to determine these types of transforms for a variety of rock and sediment types (e.g. Wyllie et al., 1956; Raymer et al., 1980). These formulations have been primarily determined for consolidated sandstones and are only applicable over small porosity ranges. The study conducted by Erickson and Jarrard (1998) on unconsolidated, high-porosity siliciclastic sediments improves on previous formulations and accurately predicts velocity over a large range of porosity. Erickson and Jarrard (1998) identified three dominant variables which affect compressional wave velocity and the presence of a critical porosity threshold (e.g. Nur et al., 1998).

In this study, a relationship between velocity and porosity for the Shikoku Basin underthrust sediments has been developed based on the global empirical velocity-porosity relation of Erickson and Jarrard (1998). The parameters from the Erickson and Jarrard (1998) normal consolidation model were used as starting parameters for a nonlinear least squares fit to the Shikoku Basin

underthrust sediments. This new formulation represents a significant improvement over previous velocity-porosity formulations for this margin (e.g. Hydman et al., 1993) and will be used in future studies to convert high-resolution 3-D marine seismic reflection data (Bangs et al., 1999; Moore et al., 1999) to porosity and pore pressure.

In addition to understanding porosity and pore pressure variations in the underthrust sediments at the Nankai Trough, important information can be learned from the physical properties of the reference site. A reference site (Site 1173, Fig. 1.2) was sampled to characterize the initial state of the sediments prior to tectonic deformation and décollement formation. The characteristics of physical properties changes at this site suggest that other factors, in addition to consolidation, play an important role in affecting the properties of the sediments. In the upper Shikoku Basin facies, porosity deviates significantly from the normal compaction trends for these types of sediments (e.g. Hamilton, 1976). Seismic velocity in this interval also deviates from the expected trend of increasing velocity with depth. At the boundary between the upper and lower Shikoku Basin facies, porosity suddenly decreases whereas there is little change in seismic velocity. In contrast, porosity and velocity values below this boundary generally follow a normal basinal compaction trend.

The physical properties data from the upper and lower Shikoku Basin sediments for Site 1173 are used to constrain the factors contributing to the high porosities in the upper Shikoku Basin facies and the abrupt physical properties changes that occur above and at the upper/lower Shikoku Basin facies boundary. Because silica diagenesis is thought to play a significant role in both

of these intervals (Shipboard Scientific Party, 2001a), the analysis is focused on the physical properties changes expected during the opal-A to opal-CT and opal-CT to quartz transitions. The high porosities in the upper Shikoku Basin facies are mostly likely caused by cementation partly related to silica diagenesis. The abrupt changes at the upper/lower Shikoku Basin boundary most likely represents the breakdown of this cementing phase. The implications for the existence of a critical porosity transition at a fractional porosity of 0.65 in the upper Shikoku Basin sediments are examined in terms of silica diagenesis and other possible diagenetic effects.

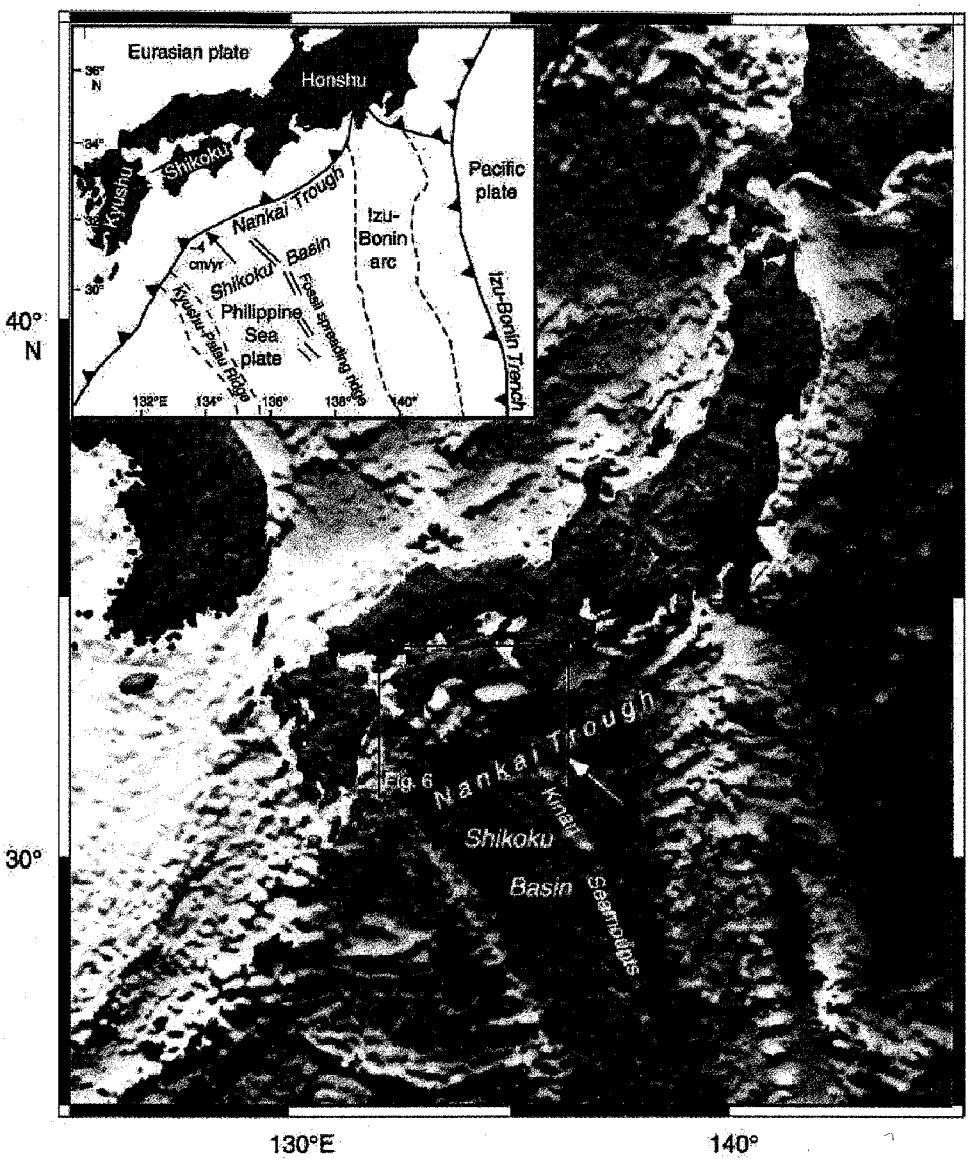

Figure 1.1: Map showing the location of the Nankai Trough. The black box outlines the enlarged section shown in Fig. 2. The convergence direction is indicated by the yellow arrow. The inset (upper left) illustrates the tectonics associated with the Nankai Trough. Shipboard Scientific Party, 2001a.

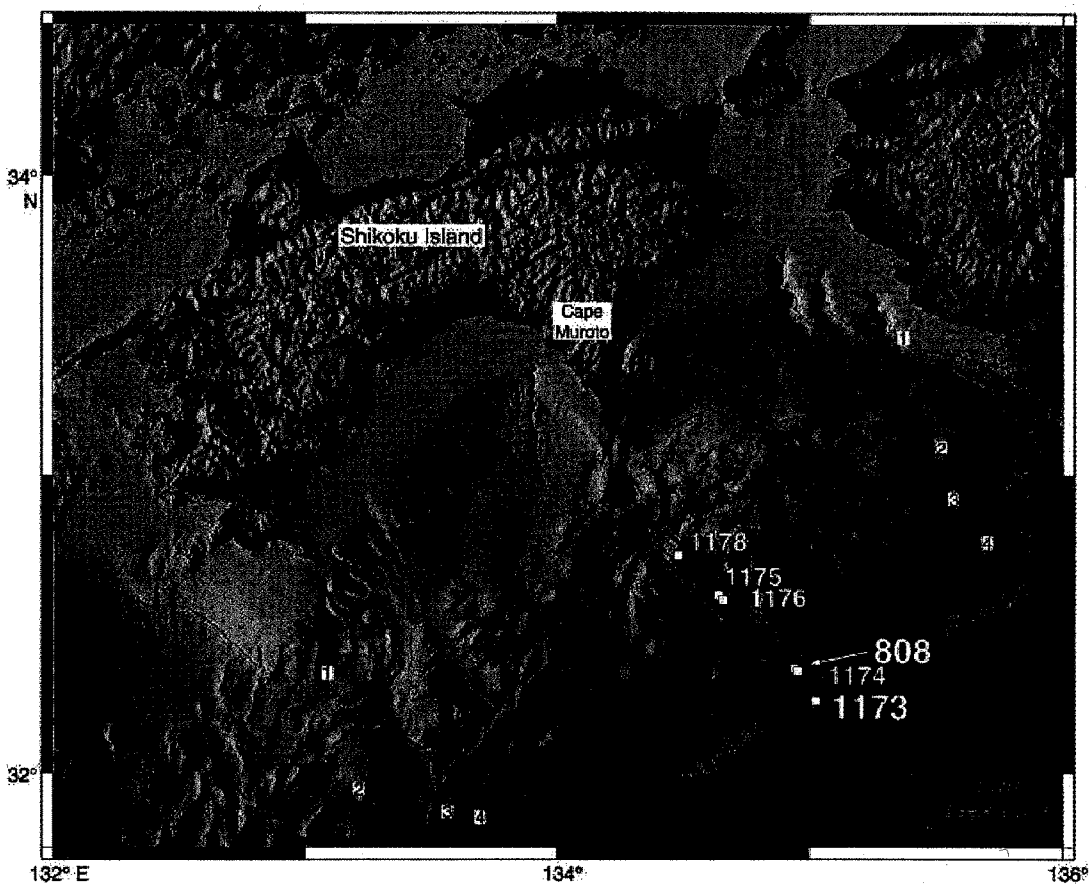

Figure 1.2: Map showing the location of ODP Sites 1173, 1174 and 808 for Legs 190 and 196. The red box outlines the location of the three-dimensional seismic survey (Bangs et al., 1999; Moore et al., 1999). The depth contours are in km. Shipboard Scientific Party, 2002a.

CHAPTER 2

BACKGROUND

2.1 Geologic Overview

The Nankai Trough is the subducting boundary between the Eurasian Plate and the Philippine Sea Plate (Fig. 1.1). The convergence rate varies between 2cm/year based on trench wedge age (Karig and Angevine, 1986) to 4 cm/year estimated from seismic slip vector (Seno, 1977). Active sediment accretion is currently taking place from a thick terrigeneous sediment section of the Shikoku Basin on the incoming Philippine Sea Plate. The trench fill sediments are approximately 500 m thick and are underlain by a 500-1000 m thick hemipelagic sediment section (Taira et al., 1989).

The Shikoku Basin was formed as a backarc basin behind the Izu-Bonin Arc during the late Oligocene to Middle Miocene (25 to 15 Ma) (Kobayashi and Nakada, 1978; Chamot-Rooke et al., 1987) about the same time as the formation of the Sea of Japan. Widespread igneous activity within the fore-arc between 17-12 Ma is generally interpreted as the initial subduction of the young Shikoku Basin seafloor and the formation of the Nankai Trough (Kano et al., 1991). The collision of the Izu-Bonin Arc and the Japanese Island Arc produced uplift of the central Japan mountain range and serves as a main sediment source for the trench with a sedimentation rate in the trough exceeding 1 km/Ma (Shipboard Scientific Party, 1991a).

The Tertiary-Cretaceous Shimanto Belt in an on-land example of an older accretionary prism. It is characterized by imbricated thrust sheets of trench turbidites and melanges composed of ocean-floor basalt, pelagic limestone, radiolarian chert, and hemipelagic shale intermixed with highly sheared scaly shale (Taira et al., 1988). The youngest part of the Shimanto belt was formed by plate subduction along the eastern margin of the Asian continent before the opening of the Japan Sea. The Shimanto Belt is interpreted as a direct analog of the Nankai accretionary prism based on the age of the subducted lithosphere, trench turbidite thickness, structural features and burial depth.

2.2 Previous Studies

The Nankai Trough is an excellent location for the study of a clastic prism. Substantial site survey data is available including high-quality 2-D and 3-D seismic reflection surveys, bathymetry, side-scan sonar, and heat flow analyses. The Nankai Trough has also been the focus of Deep Sea Drilling Project (DSDP) Legs 31 and 87 and Ocean Drilling Program (ODP) Legs 131, 191, and 196 (Fig. 1.2).

DSDP Legs 31 and 87 focused on the structural evolution of the Nankai prism (Shipboard Scientific Party, 1991a). The main focus of ODP Legs 131, 190 and 196 was to acquire in-situ measurements of the sediment physical and mechanical properties. As the first part of a two-leg program, Leg 190 specifically concentrated on coring and sampling a series of sites across the prism within a three-dimensional (3-D) seismic reflection survey (Shipboard Scientific Party, 2001a). Leg 196 sites were drilled to measure in-situ physical properties and begin long term monitoring of the initial deformation zone

(Shipboard Scientific Party, 2002a).

2.3 Structural Description

Along the Muroto transect, the Nankai accretionary prism is divided into the following tectonic/structural domains based on 3-D multi-channel seismic data (Moore et al., 2001; Fig 2.1): Nankai Trough trench axial zone, protothrust zone, imbricate thrust zone, frontal out-of-sequence thrust zone, large thrust-slice zone and landward-dipping reflector zone. The main focus of drilling at Sites 1173, 1174 and 808 was to characterize the initial state of the incoming sediments and how they are altered during initial accretion, deformation and décollement formation. In accord with this, only the trench axial zone, protothrust zone, and the imbricate thrust zone will be described in greater detail.

The trench axis of the Nankai trough is composed of a thick seaward-thinning wedge of trench turbidites that overlie the Shikoku Basin hemipelagic sediments (Moore et al., 2001). The turbidites have been transported laterally along the axis of the trough from the mountain ranges of the arc-arc collision zone (Taria and Niitsuma, 1986; Taira et al., 1991). Site 1173, located approximately 11 km seaward of the deformation front, was drilled into basement seaward of the trench fill sediments in order to provide a reference site for the physical properties of the incoming sediments.

Further landward, the protothrust zone is located between the deformation front and the frontal thrust zone. This zone is characterized by initial sediment deformation and development of the décollement in the hemipelagic

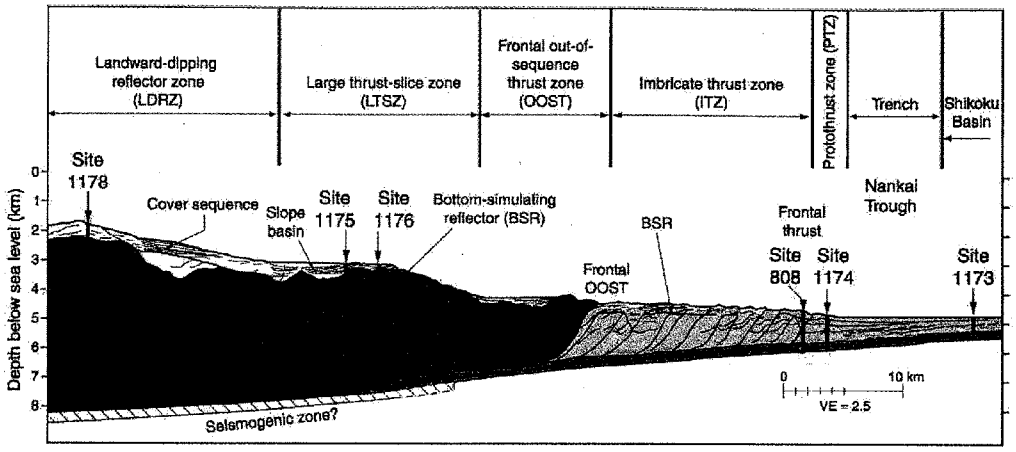

Figure 2.1: Cross-section showing major structural features based on seismic reflection data from Hills et al. (2001). Site 1173 is used as the reference site where there is little or no tectonic deformation in the sediments. Shipboard Scientific Party, 2002a.

unit (Moore et al., 2001). Site 1174 was drilled through the subducting sediments into basement and was chosen to sample across the protothrust, décollement and underthrust sediments.

Landward of the protothrust zone is the imbricate thrust zone which consists of a series of seaward-vergent imbricate thrusts spaced several kilometers apart (Moore et al., 2001). The thrusts end as a well defined décollement above the oceanic crust. This 20 km wide zone is bounded on the seaward side by the frontal thrust zone where Site 808 was drilled through the décollement into basement in order to obtain data in the frontal thrust, décollement, and underthrust zones near the deformation front.

CHAPTER 3

SITE DESCRIPTIONS

3.1 Site 1173 Lithostratigraphy

Site 1173 was drilled to define the predeformation state of the incoming sediments and to serve as a reference for additional sites further landward. Site 1173 has been divided into four lithostratigraphic units (Fig. 3.1) which can be correlated to Sites 1174 and 808: trench-wedge facies, upper Shikoku Basin facies, lower Shikoku Basin facies, and volcaniclastic facies (Shipboard Scientific Party, 2001b). The following lithostratigraphic description is summarized from Shipboard Scientific Party (2001b).

The trench-wedge facies (0-102 mbsf) is Quaternary in age and can be further divided into two subunits. The upper subunit is a silty clay interbedded with silt, silty sand, sandy silt, and rare beds of volcanic ash. The composition of this subunit is consistent with deposition on the outer trench floor. The lower subunit is transitional between the trench-wedge facies and the upper Shikoku Basin facies and is composed of silty clay with scattered interbeds of volcanic ash. The depositional environment is consistent with hemipelagic settling and includes sporadic influxes of pyroclastic particles and siliciclastic turbidites.

The Upper Shikoku Basin sediments (102-344 mbsf) are Pliocene to Quaternary in age. The composition varies between silty clay and clayey silt and with increasing compaction becomes silty claystone and clayey siltstone.

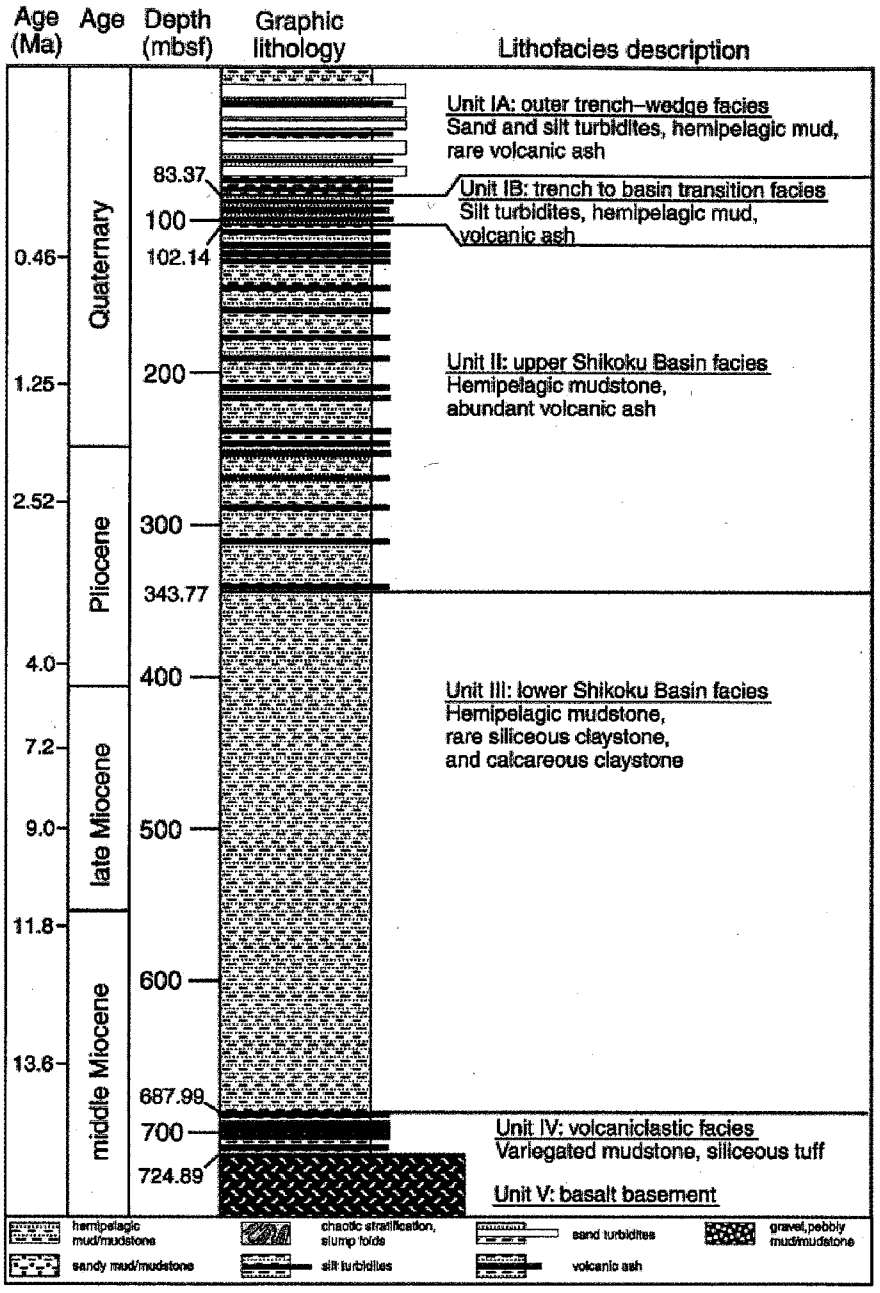

Figure 3.1: Stratigraphic column for Site 1173. The proto-décollement is located between ~390 mbsf (meters below seafloor) and 420 mbsf. Shipboard Scientific Party, 2001b.

Interbedded volcanic ash layers are common, ranging in thickness from 1-2 cm up to 25 cm, with many beds 5-15 cm thick. These sediments were deposited by hemipelagic settling with interruption by pyroclastic particle settling from air falls.

The lower Shikoku Basin sediments (344-688 mbsf) are Pliocene to middle Miocene in age and are a typical hemipelagic deposit consisting predominantly of silty claystone with scattered carbonate-cemented intervals in the middle and lower sections of the unit.

The volcanciclastic unit (688-725 mbsf) is composed of siliceous claystone and silty claystone of middle Miocene age. The silty claystone is a hemipelagic deposit while the siliceous claystone appears to be an altered volcaniclastic deposit. Immediately beneath the volcanciclastic unit is basalt of middle Miocene age, by analogy to basalt from Site 808.

3.2 Site 1173 - Deformation

Deformation features at Site 1173 are not common, which is consistent with this site being chosen as a reference site for the other locations along the Muroto transect. The deformation features that are present include bedding dips, zones of breccia and microfractures (Shipboard Scientific Party, 2001b). The majority of these features are concentrated in the upper and lower Shikoku Basin facies. The following description of the deformation features is summarized from Shipboard Scientific Party (2001b).

Based on core data from Leg 190 Hole 1173A, bedding dips up to 25° with a general north-south strike are present between ~325 to 550 mbsf (upper

and lower Shikoku Basin facies). Using RAB (resistivity-at-bit) images from Leg 196 Holes 1173B and 1173C, bedding dips greater than $\sim 5°$ were observed between 50-200, 280-560, 600-720 mbsf.

Microfaults and fractures were predominantly observed in the upper and lower Shikoku Basin facies. Microfaults with normal displacement on the order of 2-10 mm are present between 250 and 275 mbsf. There is also a ~30 cm zone of foliated breccia and high angle faults at ~440 mbsf. Fracturing was identified between 80-200, 320-570, 660-700 mbsf with the highest concentration between 380-520 mbsf. The majority of the fracture dips are between $50° - 70°$. When displacement could be determined, it was normal and of the order of 10-20 cm.

The deformation features observed at this site are generally consistent with lateral extension, due to vertical compaction and burial (Shipboard Scientific Party, 2001b). Understanding and characterizing the deformational features at the reference site is necessary in order to compare with the more highly deformed sites further landward. Specific features which are the result of deformation within the prism can then be more easily identified.

3.3 Site 1174 - Lithostratigraphy

Site 1174 is located in the protothrust zone and was designed to sample the zone of initial deformation and décollement formation. There are five lithostratigraphic units recognized at this site (Fig. 3.2) which can be correlated to Sites 1173 and 808: slope-apron facies, trench-wedge facies, upper Shikoku Basin facies, lower Shikoku Basin facies, and volcanciclastic facies (Shipboard

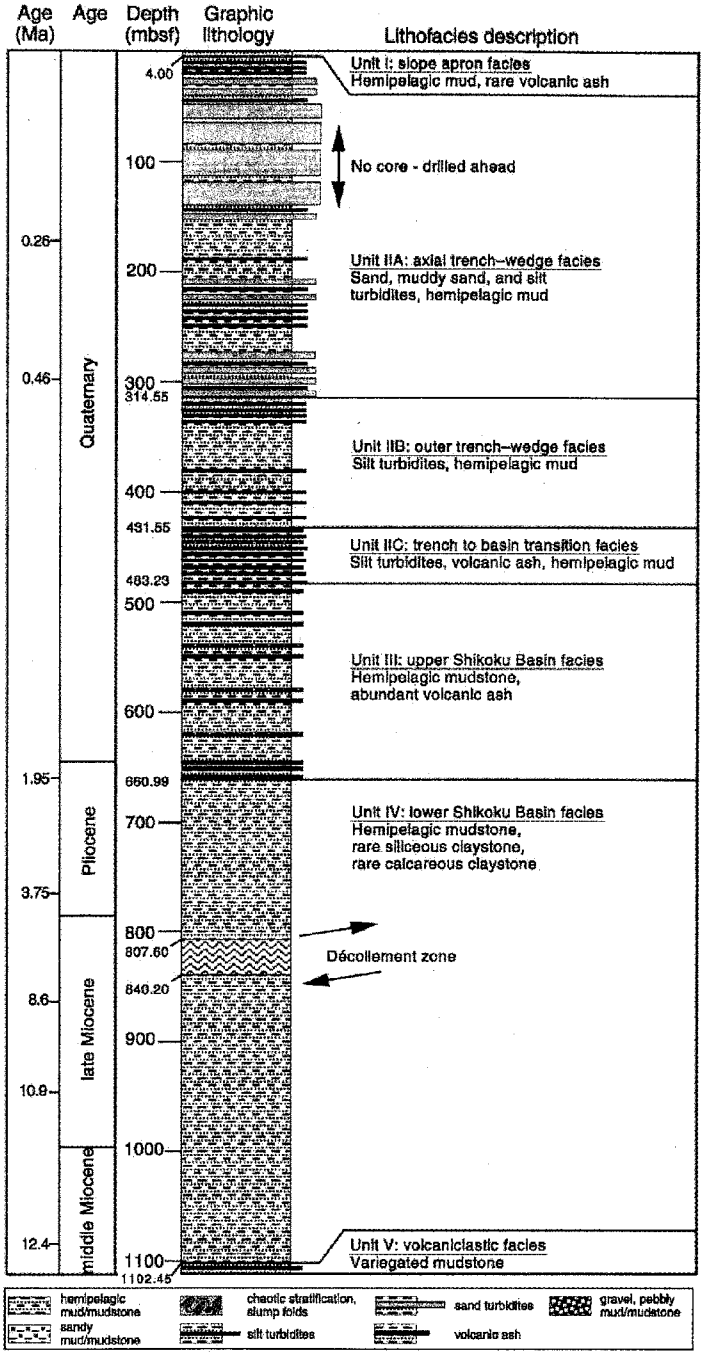

Figure 3.2: Stratigraphic column for Site 1174. The décollement is located between 808 and 840 mbsf. Shipboard Scientific Party, 2001c.

Scientific Party, 2001c).

The slope-apron facies (0-4 mbsf) is composed of silty clay to clayey silt with a single 22 cm-thick glass-rich ash layer at 3.38 mbsf. This unit was deposited by hemipelagic settling and possibly muddy turbidity currents.

The trench-wedge facies (4-483 mbsf) is broken down into three subunits: the axial trench-wedge facies, outer trench-wedge facies, and the trench to basin transition facies. The axial trench-wedge facies (thickness $\sim$ 310 m) is composed of sand, silty to muddy sand, silt to sandy silt, silty clay to clayey silt, and one thin bed of volcanic ash. The depositional environment is consistent with deposition in the axial portion of the trench wedge. The lower subunits - outer trench-wedge facies (315-432 mbsf) and the transition facies (432-483 mbsf)) are both equivalent to the corresponding units at Site 1173.

The upper (483-661 mbsf) and lower (661-1102 mbsf) Shikoku Basin facies at this site are also equivalent to the corresponding units at Site 1173. The boundary between these two units appears to be controlled by diagenesis as at Sites 1173 and 808.

The volcanciclastic facies begins at 1102 mbsf and consists of 8.86 m of variegated silty claystone.This unit likely represents the top of the volcanciclastic facies at Site 808 (Shipboard Scientific Party, 1991b).

3.4 Site 1174 - Deformation

The deformation features at Site 1174 are consistent with initial deformation in the prism sediments. The important features at this site include: deformation bands, fracture zones, steepened bedding zones, the basal

décollement zone, and the little deformed underthrust section (Shipboard Scientific Party, 2001c).

Deformation bands are primarily concentrated between 218 mbsf and 306 mbsf. When displacement along the band could be determined it was in the reverse direction. The sheared zone at 306 mbsf is 35 cm thick and is characterized by a foliated breccia and a distinctly inclined fabric. Reverse movement, orientation of fold axial planes, and inclined fractures suggest the structure is possible a backthrust within the prism.

The protothrust domain is characterized by irregularly spaced zones of fractured or brecciated rock or steepened bedding dips between 463 mbsf and 504 mbsf. Deeper intervals of fractures and brecciation are located between 688 mbsf and 807 mbsf (top of the décollement). The zones range between 10-90cm in thickness and are separated by many meters of intact material.

Core-scale faults are most common between ~495 mbsf and 611 mbsf. They are no more than one or two millimeters in diameter with normal displacements of approximately a millimeter to a centimeter. These faults are more commonly developed than at Site 1173 but less so than at Site 808. Their apparent random orientation probably reflects the effects of greater burial depth and compaction.

The top of the décollement is marked by the onset of distinctive inclined fractures. This zone is generally characterized by trapezoidal blocks which decrease downward in size to brecciated material. The base of the décollement is marked by a contact between an interval of finely broken sediments and intact sediment below. The décollement zone has a a vertical thick-

ness of 32.6 m. The underthrust sediments show some evidence of localized tectonic deformation and early compaction processes but are generally undeformed.

3.5 Site 808 - Lithostratigraphy

Site 808, drilled in the frontal thrust of the imbricate thrust zone, is broken down into the following lithostratigraphic units (Fig. 3.3): slope apron deposits, trench-fill facies, trench-basin transition facies and the Shikoku Basin facies (Shipboard Scientific Party 1991b,2002c).

The lower slope apron deposits (0-20.55 mbsf) extend from the seafloor to the first thick sand bed. This unit is composed of interlayered clayey silt and fine-grained sand, clayey silt, sandy clayey silt and very thin ash layers. These sediments were deposited through large-scale downslope sliding of semi-consolidated sediments. The sands may have been deposited by either turbidity currents or axial flows. This unit corresponds to the slope apron facies at Site 1174 but are not present at Site 1173.

The trench-fill sediments (20.55-556.8 mbsf) correspond to the trench-wedge facies at Site 1174 and the outer trench-wedge facies at Site 1173. The Site 808 sediments are divided into the same three subunits present at Site 1174 and have similar lithologies.

The trench-basin transition facies (556.8-618.47 mbsf) corresponds to the lowest subunit of the trench-wedge facies at Site 1174 and the trench to basin transition facies at Site 1173. The Site 808 sediments are composed of clayey siltstone/silty claystone with interbedded ash/tuff layers up to 25 cm in

thickness. Very thin/thin-bedded siltstone turbidites also occur sporadically.

The Shikoku Basin facies (618.47-1243.0 mbsf) can be further subdivided into the upper and lower units and correspond to the upper and lower Shikoku Basin sediments at Sites 1173 and 1174. The boundary between the upper and lower facies is marked by the disappearance of the abundant ash/tuff layers.

Immediately beneath the Shikoku Basin facies is an acidic volcaniclastic unit lying directly on basaltic basement. This unit is composed of a variety of volcanic tuffs varying from very thin to thick-bedded and suggests deposition during an extra-basinal volcanic episode.

3.6 Site 808 - Deformation

Site 808 was drilled through the frontal thrust and the décollement zone into oceanic basement. At this site an increase in deformation and fracturing occurs relative to Sites 1173 and 1174. The major zones of deformation are the frontal thrust zone (~400 mbsf), a major fractured interval (~560 mbsf), and the décollement zone (~940-960 mbsf; Shipboard Scientific Party 1991b, 2002c).

The frontal thrust zone (~389-414 mbsf) is the most strongly deformed interval at this site and is characterized by east-northeast – west-southwest oriented fractures with steep dips ranging from 25° to 90°. The fractured interval between 559-574 mbsf has similar characteristics to the frontal thrust zone with east-northeast – west-southwest fractures dipping steeply to the south.

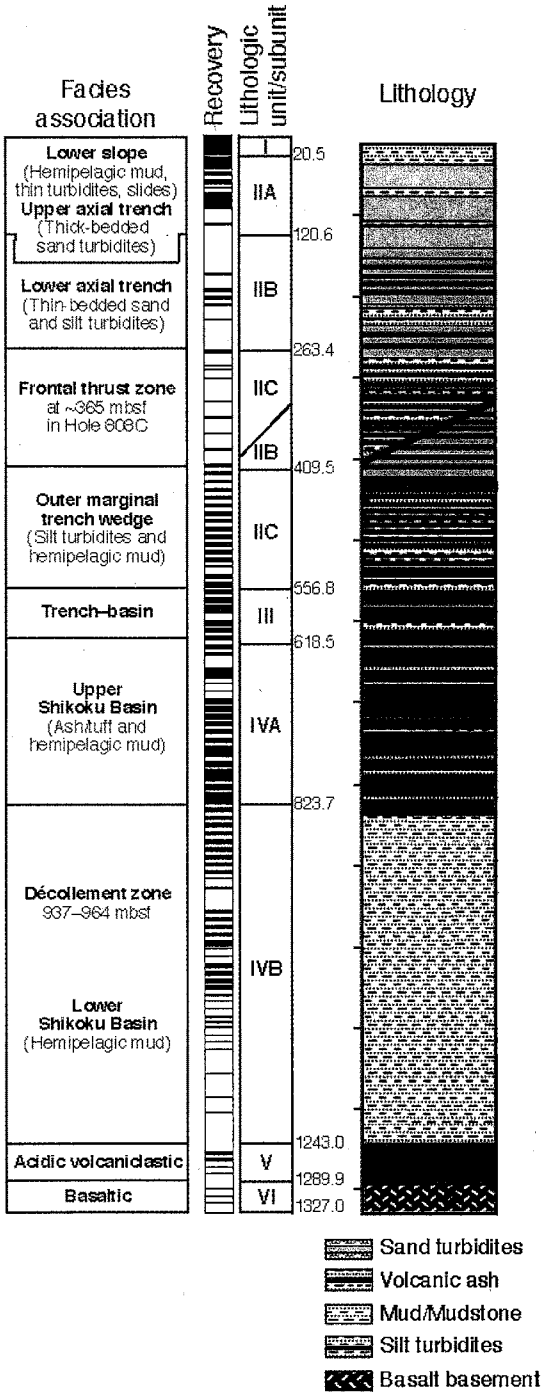

Figure 3.3: Stratigraphic column for Site 808. The décollement zone is located between 937 mbsf and 964 mbsf. Shipboard Scientific Party, 2002c.

The décollement zone in general consists of deformed intervals separated by undeformed sediments between 897-965 mbsf. The three fractured intervals between 897-904, 937-942, 959-965 mbsf are characterized by brecciation, a high concentration of faults and an increase in bedding dip. The base of the décollement is well defined by an abrupt decrease in brecciation and a decrease in the number of fractures. Physical property changes also mark this transition with a sharp increase in density and a reduction in porosity. The upper bound of the décollement is more difficult to determine and may be defined as either the top of the entire deformed interval (897 mbsf) or as the top of one of the deeper deformed intervals. Based on Leg 131 cores, the top is marked by the abrupt onset of a well-developed brecciated zone and a sharp increase in the number of faults at about 945 mbsf. From Leg 196 RAB images, the décollement zone is extended to include the interval from 937-965 mbsf based on the increase in fracture density and variations in the physical properties of the sediments. The difference where the top is defined may be explained by the 107 m offset between the two holes.

CHAPTER 4

PHYSICAL PROPERTIES DATA

A combination of core-based and logging measurements were made at Sites 1173, 1174 and 808 to characterize the downhole physical properties of the sediments along the Muroto transect. The properties measured include: magnetic susceptibility, gamma ray attenuation, P-wave velocity, S-wave velocity, natural gamma ray emissions, thermal conductivity, electrical conductivity, shear strength, and moisture and density measurements (Shipboard Scientific Party, 2001d). The following description of the physical properties data will focus on the seismic velocity and porosity.

Cores were collected for the entire drilled interval at Sites 1173 and 1174 (Leg 190) and 808 (Leg 131). Limited wireline logs were collected during Leg 190 for Site 1173. Logging while drilling (LWD) measurements were collected during Leg 196 for Site 1173 and part of Site 808.

4.1 Core measurements

4.1.1 Porosity Data

Porosity values for sediments from Sites 1173, 1174 and 808 were obtained from shipboard laboratory measurements of moisture and density made on core samples. Wet mass, dry mass, and dry volume were measured on split core specimens. Moisture content, grain density, bulk density, and

porosity were then calculated from the measured wet mass, dry mass and dry volume values as described by Blum (1997). Measurements were taken from cores collected at approximately 1-meter intervals for Sites 1173 and 808 and 2-meter intervals for Site 1174.

4.1.2 Velocity Data

Shipboard laboratory measurements of compressional wave velocity were made on core samples from Sites 1173, 1174 and 808. For unconsolidated sediments, probes were inserted into the split cores to measure transverse and longitudinal velocity. For consolidated sediments, measurements were made on 8 cm cubic samples using a Hamilton frame velocimeter contact probe system (Boyce, 1976; Hamilton, 1965). Velocity was measured in the x-, y- and z-directions (where z is parallel to the long axis of the whole-round core section). For sediments that were neither consolidated enough to cut into cubes nor soft enough to insert the transducer probes, the Hamilton frame system was used to measure velocity in the x-direction only. Measurements were taken from cores collected at approximately 3-meter intervals for Site 1173, 4-meter intervals for Site 1174, and 1.5-meter intervals for Site 808.

4.2 Wireline Logs

Wireline data was collected at Site 1173 using the triple combination tool (triple combo) and the Formation MicroScanner sonic (FMS-sonic) tool (Schlumberger, 1989). As a result of poor hole conditions, wireline log data was only collected between 65 mbsf and 362 mbsf.

4.2.1 Density and Porosity

The triple combo tool includes the hostile environment lithodensity sonde (HLDS) which measures bulk density using a ^{137}Cs radioactive source and two gamma ray detectors (Shipboard Scientific Party, 2001d). The number of gamma rays detected is directly related to the bulk density. From bulk density, porosity can be calculated by

$$\phi = \frac{\rho_{\mathrm{gr}} - \rho_{\mathrm{b}}}{\rho_{\mathrm{gr}} - \rho_{\mathrm{w}}} \tag{4.1}$$

where ρ_{gr} is the mean grain density (typically 2.7 g/cm^3), ρ_w is the pore water density (1.03 g/cm^3 for seawater), and ρ_b is bulk density measured by the HLDS tool.

4.2.2 Velocity

The dipole shear sonic imager (DSI) uses a combination of monopole and dipole transducers to measure sonic wave propagation (Shipboard Scientific Party, 2001d; Schlumberger, 1995). The DSI tool can measure both compressional and shear velocities over a range of lithologies. The wireline DSI data has been reprocessed by Goldberg (2003) using a phase picking method to improve the quality of the P- and S-wave logs.

4.3 Logging While Drilling (LWD) Logs

Logging while drilling (LWD) measurements are made shortly after the hole is drilled and before the hole deteriorates due to continued drilling and coring (Shipboard Scientific Party, 2002d). The LWD tools of interest for Leg

196 Sites 1173 and 808 are the azimuthal density (ADN) tool and the sonic while drilling (ISONIC) tool.

4.3.1 Density and Porosity

Bulk density measurements were acquired using the ADN tool which consists of a 1.7-Ci ^{137}Cs gamma ray source and two scintillation receivers located 5 and 12 inches below the source (Shipboard Scientific Party, 2002d). The number of Compton scattering collisions is related to the formation density in the borehole. Density measurements are collected every 15 cm and are then converted to porosity using the same method as for the wireline bulk density log (Eq. 4.1).

4.3.2 Velocity

Velocity data was collected with the ISONIC tool which records monopole acoustic waveforms (Shipboard Scientific Party, 2002d) and is similar to the wireline sonic array tool described earlier. Waveforms are recorded at four receivers located 10 ft, 10.67 ft, 11.33 ft, and 12 ft above the source. At least two depth points each composed of eight stacked waveforms were measured over every 30 cm interval (Goldberg at al., 2003).

The first processing attempt on the ISONIC data included bandpass filtering, restacking, waveform slowness-time coherency analysis, and depth-time merging (Shipboard Scientific Party, 2002d). For unconsolidated marine sediments, the P-wave velocity is extremely low and close to the fluid velocity making it difficult to determine an accurate velocity (Goldberg et al., 2003). The initial processing attempt did not accurately determine the P-wave veloci-

ties and additional analysis was required. Goldberg et al. (2003) and Yoneshima et al. (2003) reprocessed the raw waveforms using high-resolution dispersion analysis and the leaky-P mode, respectively. Each analysis resulted in improved P-wave velocities but the ISONIC velocity data still requires additional improvements. The Yoneshima et al. data set was available and was used for the LWD ISONIC data at Sites 1173 and 808 (Figs. 4.1 and 4.3).

4.4 Site 1173 Physical Properties

4.4.1 Porosity

Core porosities are $\sim$ 60% at 100 mbsf and increase slightly within the upper Shikoku Basin facies to $\sim$ 68% at $\sim$340 mbsf. This slight increase in porosity is a significant deviation from normal compaction trends for silty clays (e.g. Hamilton, 1976). Between $\sim$320 mbsf and 340 mbsf the porosity drops sharply to $\sim$ 50% which is the boundary between the upper and lower Shikoku Basin facies. Below this boundary, the porosities generally follow a normal compaction trend for these types of sediments. There is little change in porosity at the approximate location of the proto-décollement zone between $\sim$390 and 420 mbsf.

Wireline porosity data (Fig. 4.1) is only available between 78-336 mbsf and is generally in agreement with the core data in this interval, though with less variability. Beginning at 102 mbsf, porosity increases from $\sim$58% to an average value of 63% by the base of the log at 336 mbsf. There are sharp decreases at 264 mbsf (54%) and 323 mbsf (50%) which roughly correspond to similar decreases in the core porosities.

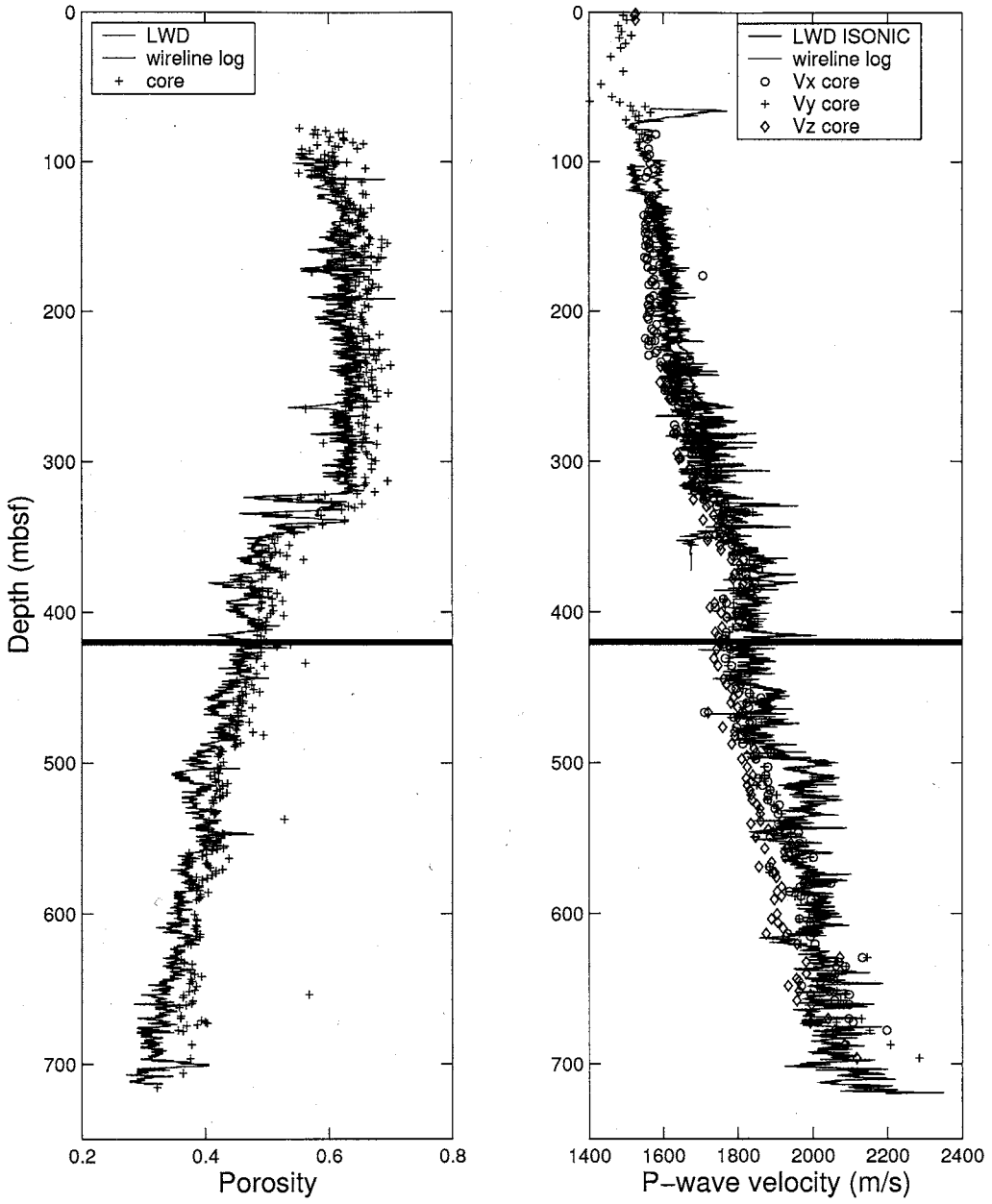

Figure 4.1: Shipboard laboratory based core, wireline log, and LWD measurements of porosity and velocity for Site 1173. The base of the décollement is indicated by the thick line.

4.4.2 Velocity

The core velocities remain relatively constant at ~1600 m/s between 83 and 230 mbsf. Velocity then increases between 230 and ~390 mbsf to ~1800 m/s. There is not a significant change in core velocity at 340 mbsf which corresponds to the sudden decrease observed in porosity. At 390 mbsf velocity decreases slightly but then smoothly increases to ~2100 m/s at the base of the hole (~700 mbsf).

Wireline compressional velocities shows similiar trends to the core velocity data. Velocities increase only slightly between 102-220 mbsf from ~1580 m/s to ~1650 m/s. At 220 mbsf velocities begin to increase at a greater rate to ~1740 m/s at 320 mbsf. Between 320 mbsf and the base of the unit at 344 mbsf, the changes become more complex. Below 330 mbsf velocity values are significantly more scattered but continue a sharp decrease to ~1650 m/s at the base of the log at 363 mbsf.

4.5 Site 1174 Physical Properties

4.5.1 Porosity

The core porosities (Fig. 4.2) decrease with depth, from 58-72% at the seafloor to 36-42% by 480 mbsf (trench to basin transition facies) (Shipboard Scientific Party, 2001c). Between 480-661 mbsf (upper Shikoku Basin facies) porosity remains essentially constant between 35% to 42% which is a significant deviation from a normal compaction trend (e.g. Hamilton, 1976). There is a decrease in porosity at the boundary between the upper and lower Shikoku Basin facies to 34%-40% which is similiar to the decrease observed at Site

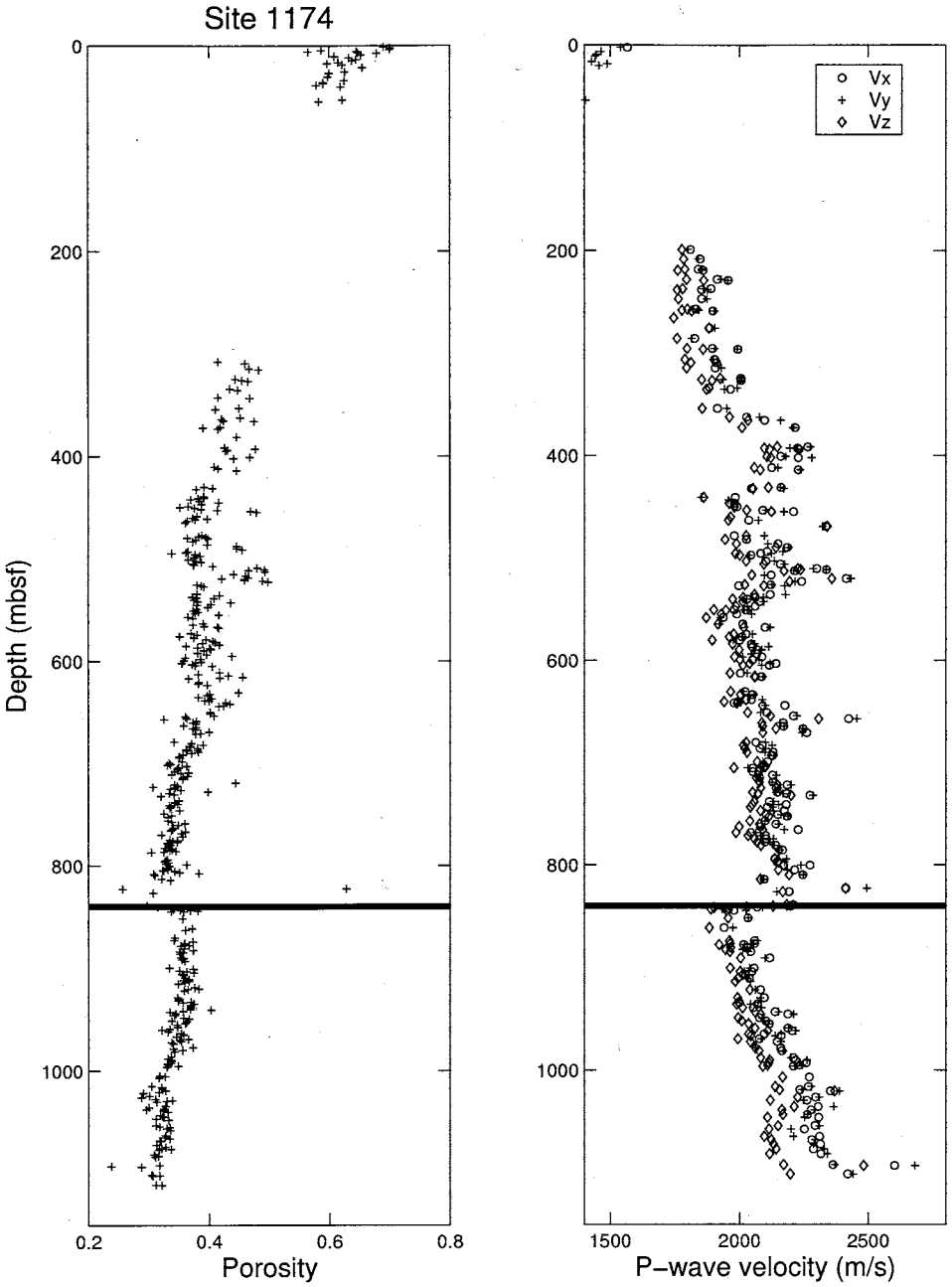

Figure 4.2: Laboratory based core measurements of porosity and velocity for Site 1174. The base of the décollement is indicated by the thick line.

1173. Porosity exhibits a normal compaction trend between 661 mbsf and 807 mbsf and decreases to 30-35% at the top of the décollement zone. Directly beneath the décollement zone (840 mbsf) porosity increases sharply. In the underthrust sediments, porosity remains relatively constant to 985 mbsf and decreases to 32-37% by the base of the hole.

4.5.2 Velocity

The core velocities (Fig. 4.2) generally increase with depth and deviate from a normal compaction curve for three intervals: between 360 and 420 mbsf, and at ~520 mbsf and ~660 mbsf (Shipboard Scientific Party, 2001c). Velocity increases abruptly between 360 and 420 mbsf to ~2100 m/s which is correlated to an interval with a higher than average cristobalite to quartz ratio (Shipboard Scientific Party, 2001c). The other two zones of high velocity (~520 mbsf and ~620 mbsf) are correlated to high silica content in the pore fluid. Velocity decreases abruptly at the base of the décollement zone which corresponds to the observed increase in porosity. In the underthrust sediments, velocity follows a normal compaction trend.

4.6 Site 808 Physical Properties

4.6.1 Porosity

The porosity values at Site 808 (Fig. 4.3) generally follow a normal compaction trend. Between 0 and ~400 mbsf porosity values fluctuate over a large range (30-70%). Between 400 mbsf and the base of the décollement at ~960 mbsf porosity decreases relatively smoothly from 40% to 25%. There is a sharp increase to ~37% at 960 mbsf beneath which porosity smoothly decreases

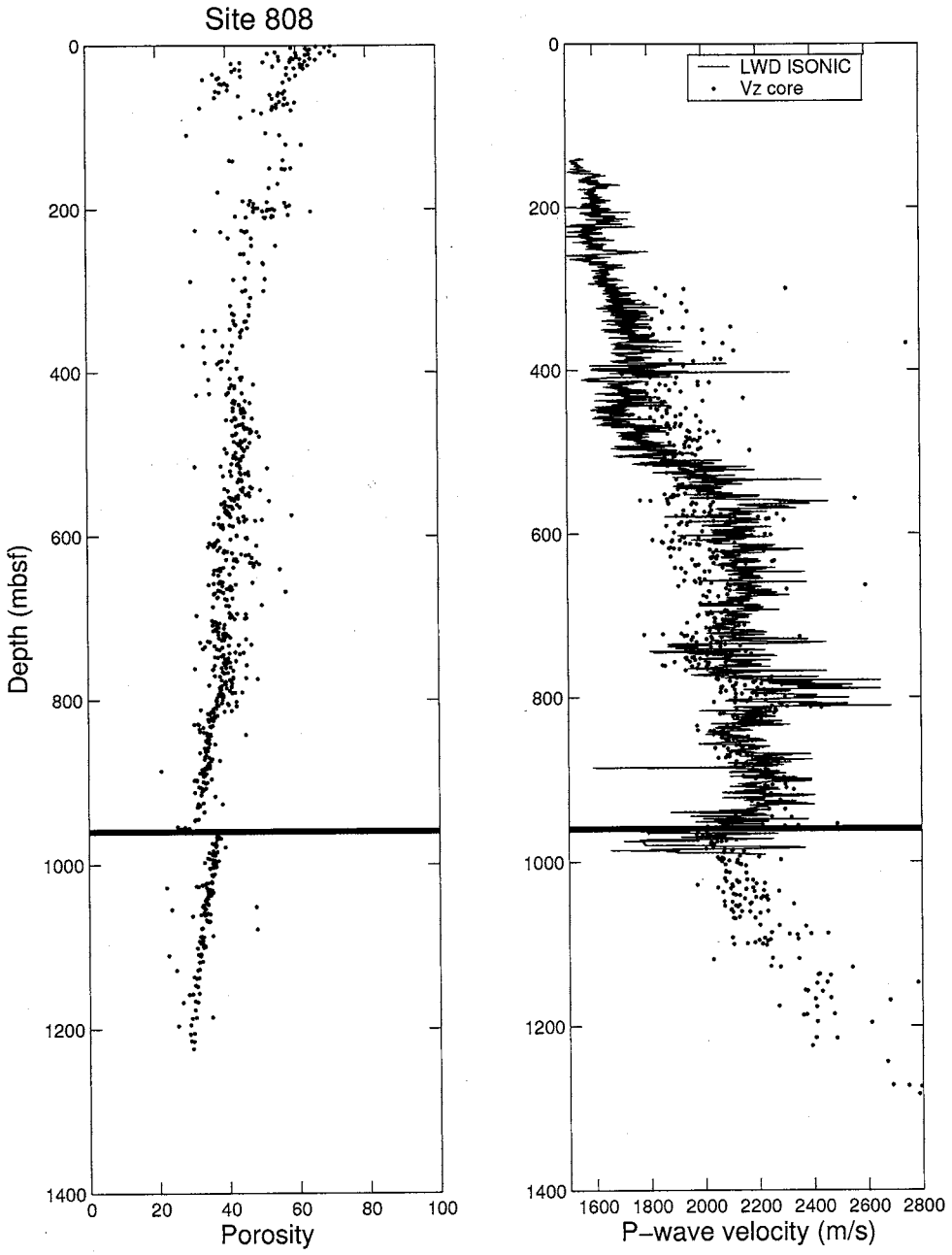

Figure 4.3: Shipboard laboratory based core and LWD measurements of porosity and velocity for Site 808. The décollement is indicated by the thick black line. Core velocities are in the vertical direction (z-direction) only. The ISONIC velocity data is from Yoneshima et al. (2003).

to ~30% by the base of the hole.

4.6.2 Velocity

The core P-wave velocity values at Site 808 (Fig. 4.3) fluctuate significantly over the entire depth of the hole. A general trend of increasing velocity with depth is observed with sharp increases at ~800 mbsf and again at the base of the décollement at ~960 mbsf. The decrease in velocity at 960 mbsf corresponds to the increase in porosity.

CHAPTER 5

VELOCITY-POROSITY RELATIONSHIP

The Shikoku Basin and Nankai accretionary prism sediments have been well imaged using seismic reflection methods (Bangs et al., 1999; Moore et al., 1999). Seismic velocity data are important for providing information about the large scale structure of the prism. Other physical properties of the sediments, such as porosity and pore pressure, are important for understanding prism hydrology, sediment mechanical properties, and deformational styles (see Shipboard Scientific Party, 2001a). A conversion between seismic velocity and porosity would provide information about regional porosity variations by allowing a conversion of marine seismic reflection data to porosity.

Numerous studies have been conducted in order to determine a relationship between compressional velocity (or acoustic velocity) and porosity for a variety of sediment and rock types. One of the earliest and most widely used transforms is the Wyllie time-average equation (Wyllie et al., 1956). This relationship is only reliable for consolidated sandstone over a small porosity range of 25% to 30% (Raymer et al., 1980). Therefore, corrections need to be made to apply this transform to unconsolidated sediments. An improved version of the time-average equation developed by Raymer et al. (1980) eliminates the need for a compaction factor correction but requires the use of a separate equation for each of three porosity ranges. As neither the Wyllie time-average equation

nor the formulation suggested by Raymer et al. adequately fit the Nankai sediments, Hyndman et al. (1993) used the results of Jarrard et al. (1989) and Han et al. (1986) to fit a smooth polynomial to Site 808 data. This fitted polynomial is applicable for a porosity range of ~30-60%.

In order to improve further on the previous studies and to determine a relationship that accurately predicts over a large range of porosity, Erickson and Jarrard (1998) completed a statistical analysis of unconsolidated, high-porosity siliciclastic sediments of the Amazon Fan to develop a global empirical velocity-porosity relationship. They identified three dominant variables affecting compressional wave velocity: porosity, shale fraction and consolidation history. A key element of their formulation is the presence of a critical porosity, or a porosity threshold, across which the relationship between velocity and porosity changes fundamentally.

5.1 Critical Porosity

Raymer et al. (1980) recognized the concept of two separate porosity domains in which velocity exhibits different behaviors. The suspension domain for high-porosity rocks describes a medium where solid particles are suspended in the fluid. The consolidated rock domain for low-porosity rocks describes a medium with a continuous framework supported matrix. Nur et al. (1998) define this transition from a suspension to a continuous matrix as the critical porosity. More importantly, the critical porosity transition divides the relationship between velocity and porosity into two domains. For porosities greater than the critical porosity, velocity is not strongly dependent on porosity. For values below the critical porosity, velocity depends strongly on

porosity and increases significantly with a small decrease in porosity.

The existence of a critical porosity transition does not indicate the transition from a zero-strength suspension to a frame-supported regime, but rather a transition where the frame modulus increases beyond a threshold and causes a substantial velocity increase (Erickson and Jarrard, 1998).

5.2 Shale fraction

Clay content was evaluated by Erickson and Jarrard (1998) as a possible third-order factor affecting compressional wave velocity. The physical dependence is indirect: clay content can affect porosity which, in turn, affects velocity. Also, lithology directly affects velocity through the matrix density and matrix velocity. By removing the effects of porosity and pressure to calculate residual velocities, Erickson and Jarrard (1998) determined that clay content has no direct influence on high-porosity sediments. They suggest for high-porosity sediments that the bulk modulus is dominated by the pore fluid modulus and lithology-dependent variations in the matrix bulk modulus are overwhelmed. However, clay content is assumed to be an important control on velocity for porosities $< 30\%$ through its direct effect on the aggregate and frame bulk moduli (Erickson and Jarrard, 1998).

Because quantitative clay content data was not generally available for their log based study, Erickson and Jarrard (1998) used an empirical "shale fraction" log which loosely predicts clay content. The shale fraction log (v_{sh}) can be calculated using the gamma ray log and the nonlinear response function for Tertiary rocks (Dresser Atlas, 1982)

$$v_{sh} = 0.083 \times 2^{((3.7*IGR)-1)} \tag{5.1}$$

where $IGR = (GR_{log} - GR_{sand})/(GR_{shale} - GR_{sand})$. The terms GR_{log}, GR_{sand}, GR_{shale} are the gamma ray (GR) log values in API units. The sand (GR_{sand}) and shale baselines (GR_{shale}) are the minimum and maximum values, respectively, in the gamma ray log.

5.3 Consolidation History

Consolidation is known to affect the compressional velocities for high-porosity sediments (Blangy et al., 1993) by not only affecting the porosity but also the shear and frame bulk moduli by increasing intergrain contacts (Erickson and Jarrard, 1998). To account for this, Erickson and Jarrard (1998) define separate velocity-porosity relationships for what are termed "normally" and "highly" consolidated sediments. These terms are empirical and not related to the soil mechanics definition of consolidation. High-consolidation is often seen with accretionary prism deformation, early cementation, or deep burial. Sedimentary basins are an example of a normal-consolidated environment.

5.4 Empirical velocity-porosity relationships

The global empirical relationships for compressional wave velocity (V_p) in terms of fractional porosity (ϕ), shale fraction (v_{sh}), and consolidation history are (Erickson and Jarrard, 1998):

Normal-consolidation (Fig. 5.1)

$$V_p = 0.739 + 0.552\phi + \frac{0.305}{(\phi + 0.13)^2 + 0.0725} + 0.61(v_{sh} - 1.123)[X_1] \tag{5.2}$$

where $X_1 = \tanh(40(\phi - \phi_c)) - |\tanh(40(\phi - \phi_c))|$ with a critical porosity (ϕ_c) of 0.31.

High-consolidation (Fig. 5.1)

$$V_p = 1.11 + 0.178\phi + \frac{0.305}{(\phi + 0.135)^2 + 0.0775} + 0.61(v_{sh} - 1)[X_2] \qquad (5.3)$$

where $X_2 = \tanh(20(\phi - \phi_c)) - |\tanh(20(\phi - \phi_c))|$ with a critical porosity (ϕ_c) of 0.39.

5.5 Velocity-porosity relationship: Shikoku Basin

In-situ corrected core-based measurements of velocity and porosity for the underthrust sediments at Sites 1173, 1174 and 808 (Figs. 4.1, 4.2, 4.3) were used to determine a velocity-porosity relationship. As core and velocity measurements were often not made at corresponding depths, velocity data was selected to within 25 cm intervals of the depths available for porosity measurements. In addition, only velocities measured in the vertical direction were used in the analysis as they correspond to seismic interval velocities.

5.5.1 In-situ Corrections

Corrections have been applied to the raw core data to account for unloading from in-situ conditions. As samples are unloaded from pressure at depth, the samples undergo a decrease in grain contact stress which causes both an increase in porosity and a decrease in seismic velocity.

Corrections to velocity and porosity values were made by comparing the core data to available wireline and LWD data at corresponding depths. Because the most complete combination of core and log data are available for

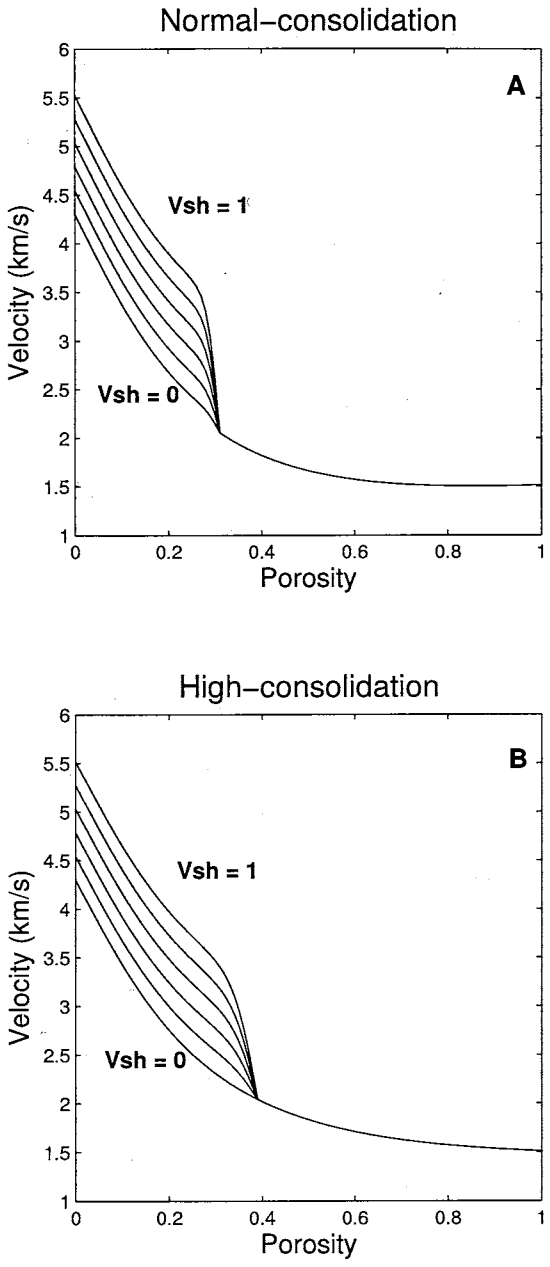

Figure 5.1: Compressional velocity as a function of porosity and shale fraction for A) normal- and B) high-consolidation (Erickson and Jarrard, 1998). Velocity is plotted for shale fractions of 0, 0.2, 0.4,0.6, 0.8, and 1.

Site 1173, this site was used to calculate the in-situ corrections applied to core measurements from Sites 1174 and 808.

Porosity correction

The Site 1173 core porosity values have been compared to both wireline and LWD porosity values. As the core and log measurements were not sampled at the same depths, a data set with matching depths was needed. Using the depths where core measurements are available, log (wireline and LWD) data was selected for depths located ± 10 cm from each core sample depth. The difference between the core and log data sets was calculated by subtracting the values at the matching depths. The difference between the core and log data appears to be near-constant with depth when comparing the core data to both the wireline (Fig. 5.2) and LWD (Fig. 5.3) data. For the core-wireline comparison, the mean fractional porosity offset is 0.0277 ± 0.0200 (core porosity is greater than log porosity). For the core-LWD comparison, the mean difference is 0.0307 ± 0.0249. Taking the average of these two values, the in-situ correction we have chosen to apply to the core data is a constant value of 0.0289 which has an error of ± 0.0224. This correction obtained from the Site 1173 data has then been applied to the core porosity data for Sites 1174 and 808.

Velocity correction

The wireline DSI data from Site 1173 is the only reliable velocity log data and has been used to determine the in-situ velocity correction. The reprocessed wireline velocities (Goldberg, 2003) have been used in this analysis. The wireline velocities deviate from a general trend of increasing velocity and

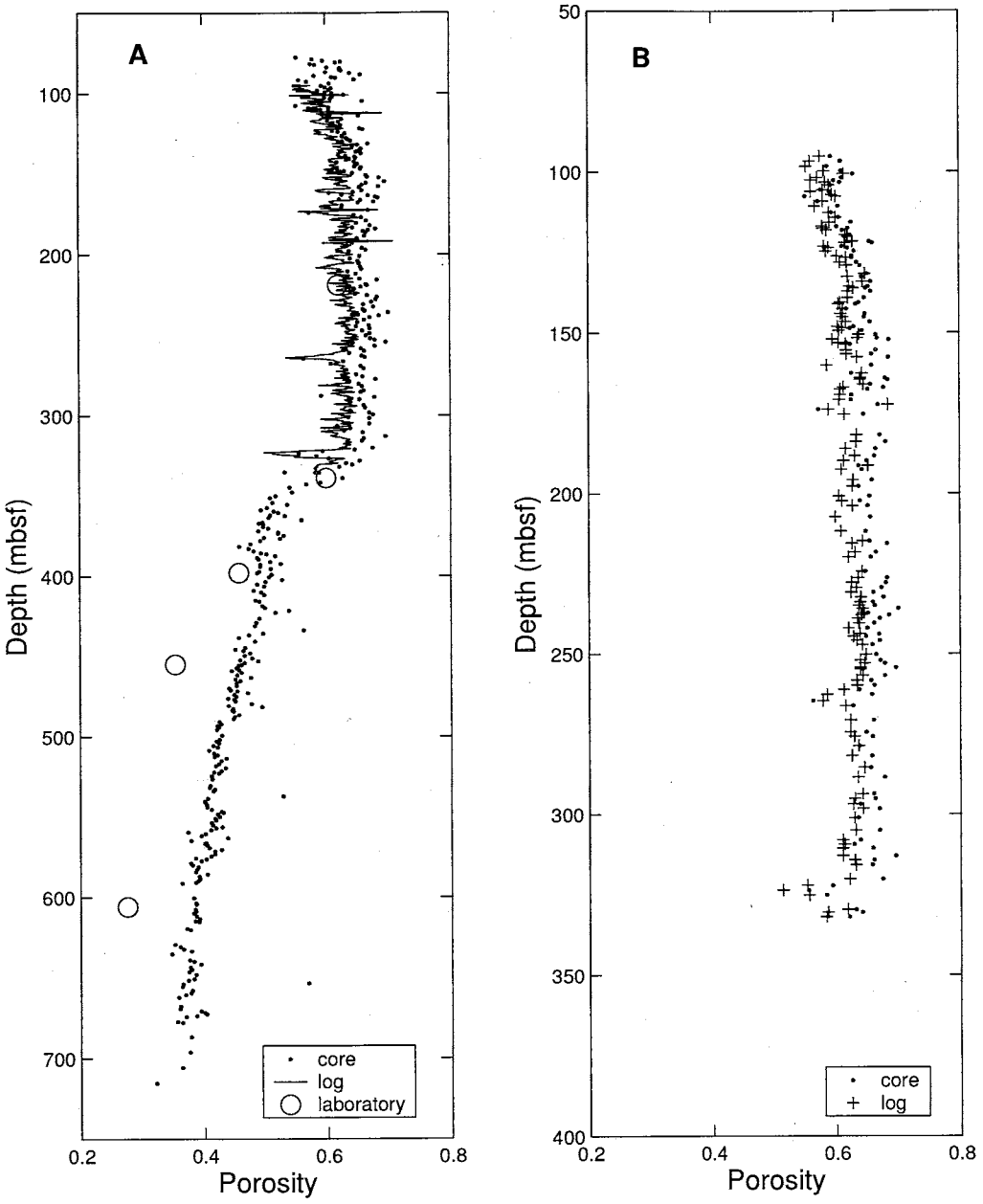

Figure 5.2: Core, wireline log, and laboratory porosity measurements for Site 1173. A) All available porosity data. B) Porosity data with corresponding depths to ± 10 cm. Laboratory data are plotted for the calculated in-situ effective pressure. (Note the change in depth scale between A and B).

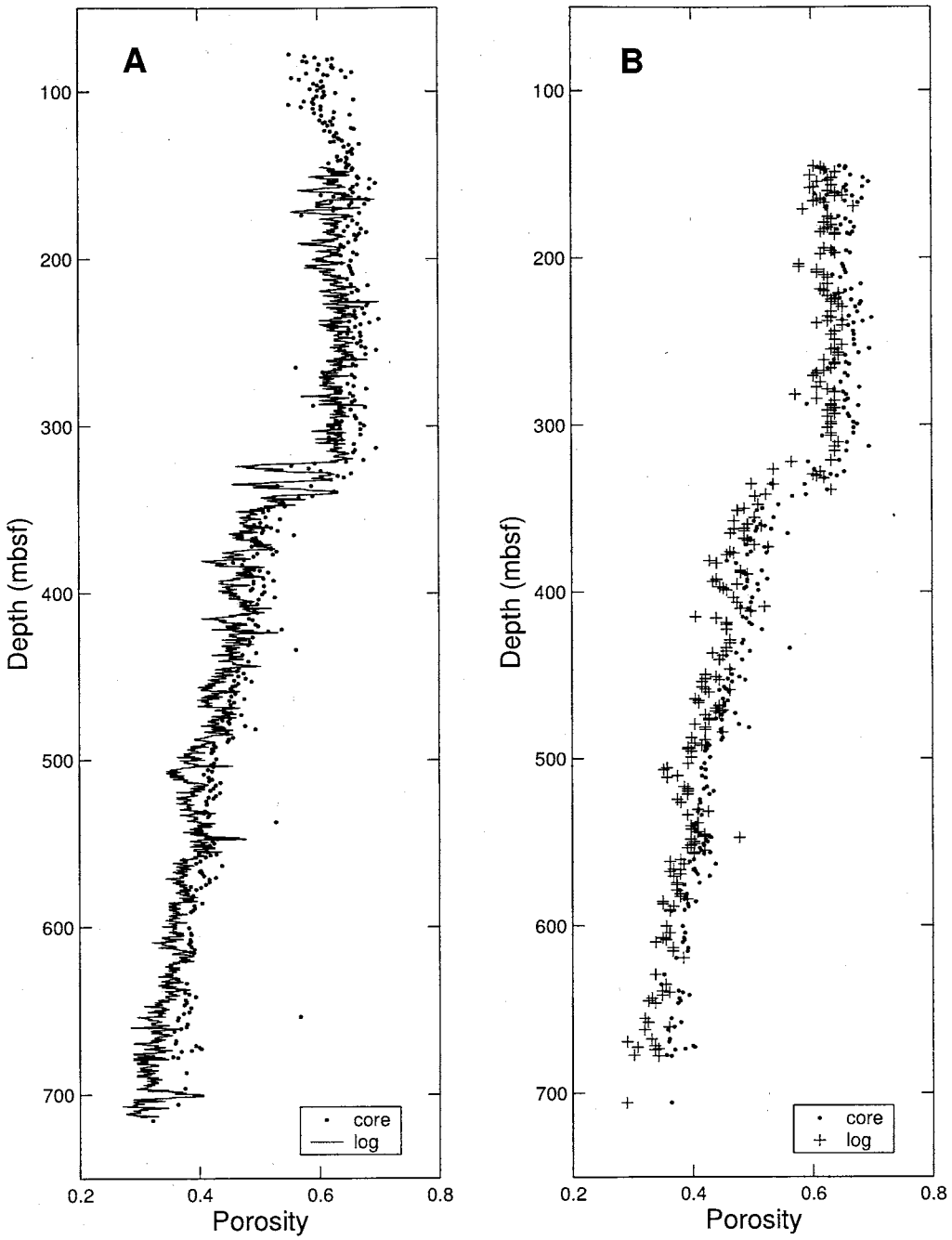

Figure 5.3: Core and LWD porosity measurements for Site 1173. A) All available porosity data B) Porosity data with corresponding depths to ± 10 cm. Laboratory measurements are not show in this figure - see Figure ??.

begin to decrease at about 345 mbsf (Fig. 5.4), which is the boundary between the upper and lower Shikoku Basin facies. Due to this change in velocity, the in-situ correction has been determined based only on the data above ~340 mbsf.

As for the porosity data sets, core velocity and log velocity measurements were not taken at the same depths. Using the same method described for the porosity correction, log data was selected for depths located ±20 cm from each core depth. The difference between the core and log data could then be calculated by subtracting the data sets at the matching depths.

The difference between the core and wireline velocities is expected to increase with depth (e.g. Hamilton, 1978); however the standard deviation of the mean difference between the data sets is too large for any depth-dependent trend to be apparent. Instead, we have chosen to use the average difference between the core and wireline velocity data of 43.39 m/s (with an error of ±29.05 m/s) as a constant in-situ correction. This correction was subtracted from the core velocity data for Sites 1173, 1174 and 808.

Laboratory Measurements

Laboratory tests on samples from Site 1173 were conducted to measure P- and S-wave velocities under confining pressures (see Appendix A). The resulting compressional wave velocity and porosity measurements can be used to compare with the in-situ corrections determined from the core-log data comparison.

The laboratory measurements of porosity generally agree with the in-

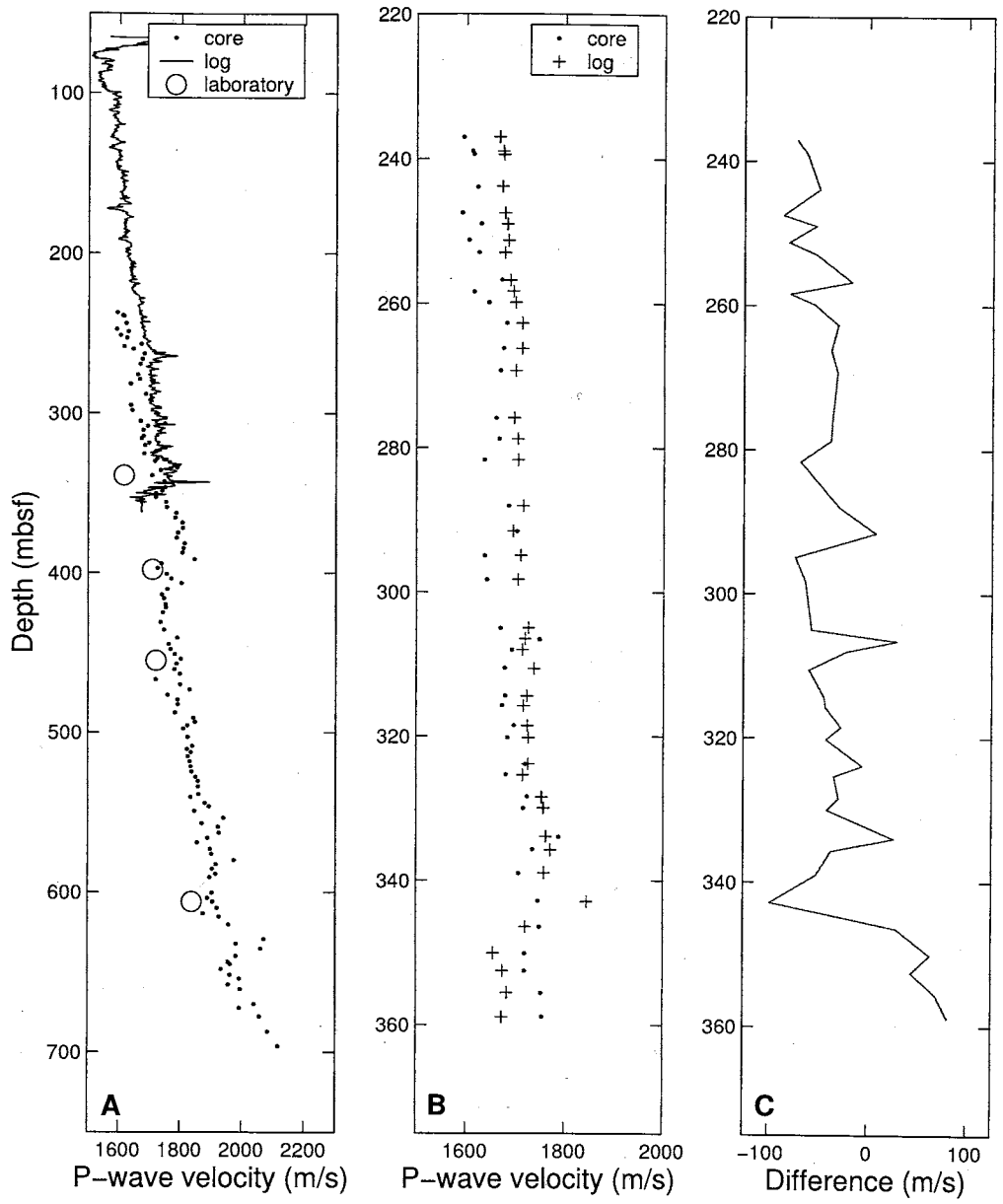

Figure 5.4: Core,wireline, and laboratory P-wave velocity measurements for Site 1173. A) all available velocity data. B) data with corresponding depths (±20 cm). C) the difference in velocity between core and wireline measurements. There is a slight trend towards decreasing offset with depth. (Note the change in depth scale between A and B).

situ correction determined above. For sediments above the décollement, laboratory measurements of porosity are an average of 3% less than the shipboard core measurements and agree with the log values at these depths (Figs. 5.2 and 5.4). Below the décollement, the difference between the laboratory measurements and shipboard core measurements increases to about 10%.

The laboratory measurements of P-wave velocity do not agree with the in-situ correction determined from the wireline log and core data comparison (Fig. 5.4). The laboratory velocity measurements are consistently lower than both the core and wireline log measurements, which is the opposite of what is expected based on the previous comparison between core and logging measurements. Further analysis of the P-wave velocities might result in values which are more realistic and agree more closely with the in-situ correction.

5.5.2 Shale fraction

Shale fraction (Fig. 5.5) was calculated for Site 1173 based on Equation 5.1 using the LWD gamma ray log. The sand and shale baselines were determined from the LWD gamma ray log for Site 808 as no "clean" sands at Site 1173 were present from which to determine these values.

5.5.3 Parameter fitting

The functional form of Equations 5.2 and 5.3 has been used to determine a velocity-porosity relationship for the Shikoku Basin underthrust sediments. New parameters were determined using an implementation of the nonlinear least-squares Levenberg-Marquardt algorithm. The starting parameters for the fitting algorithm were obtained from the normal-consolidation equa-

tion of Erickson and Jarrard (1998). Since the velocity-porosity relationship is developed for the underthrust section which is in a basinal compaction state, the normal trend was considered more appropriate than the high-consolidation trend. The parameters fit in the analysis are A, B, C, v_{sh} and ϕ_c (Eq. 5.4). The form of the equation fit using the nonlinear least-squares method is

$$V_p = A + B\phi + \frac{0.305}{(\phi + C)^2 + \frac{0.305}{1.51 - A - B} - C^2 - 2C - 1} + 0.61(v_{sh} - 1.123)[X_m] \tag{5.4}$$

where $X_m = \tanh(40(\phi - \phi_c)) - |\tanh(40(\phi - \phi_c))|$. This equation incorporates the boundary condition of V_p=1.51 km/s at a fractional porosity of 1.

5.6 Results: Velocity-porosity relationship

Velocity versus porosity is plotted for the in-situ corrected core data for all three sites (Fig. 5.6). These data are plotted for both above and below the décollement (Fig. 5.6A) and then for below the décollement only (Fig. 5.6B). The plot for data above and below the décollement does not show a significant trend of increasing velocity with decreasing porosity, except for Site 1173, whereas there is a much more obvious trend for the underthrust sediments. The bounding equations from Erickson and Jarrard (1998) for normal- and high-consolidation are also plotted for the underthrust sediments (Fig. 5.7). The underthrust data lie mostly within the bounds of these equations but follow the normal consolidation trend more closely.

The fitted parameters are listed in Table 5.1, which includes the sensitivity of the fit to each parameter. The RMS of the residuals for these parameters is ±73.34 m/s. The best-fit formulation is plotted in Figure 5.7.

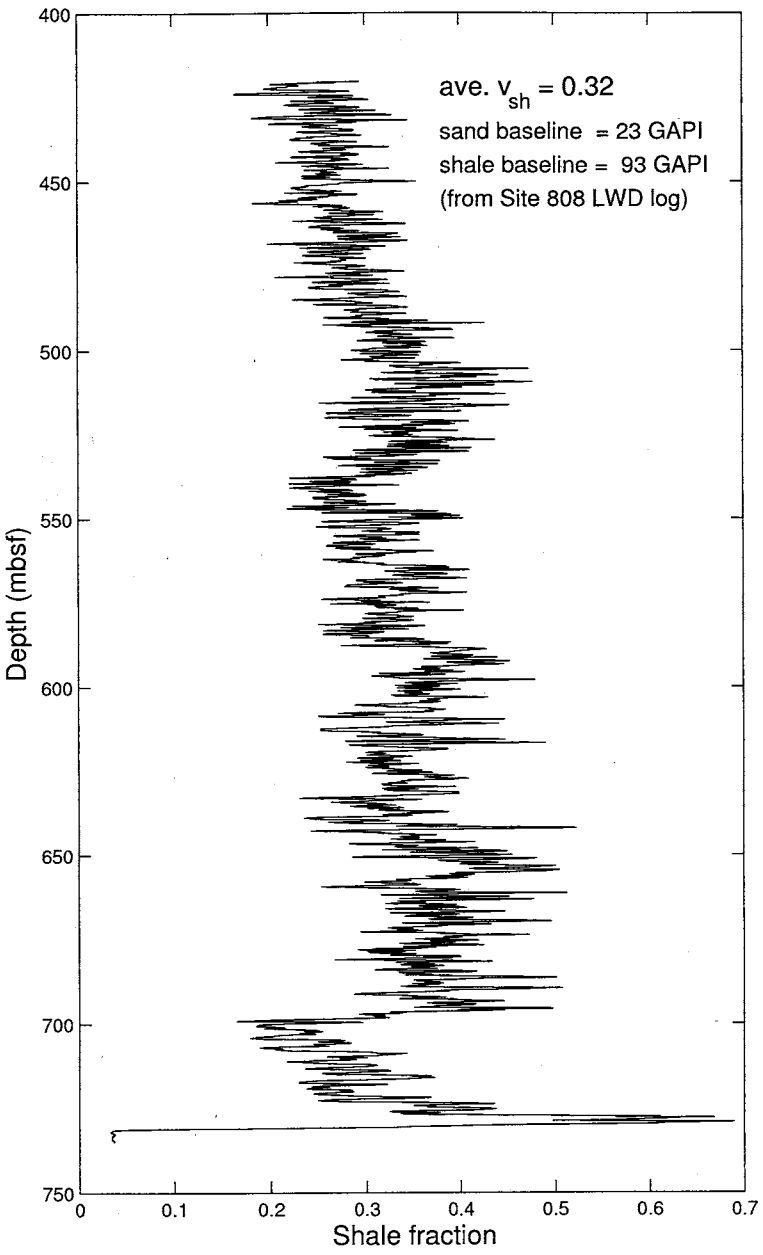

Figure 5.5: Calculated shale fraction log for Site 1173. The average shale fraction is 0.32. The sand and shale baselines were taken from the LWD gamma ray log from Site 808.

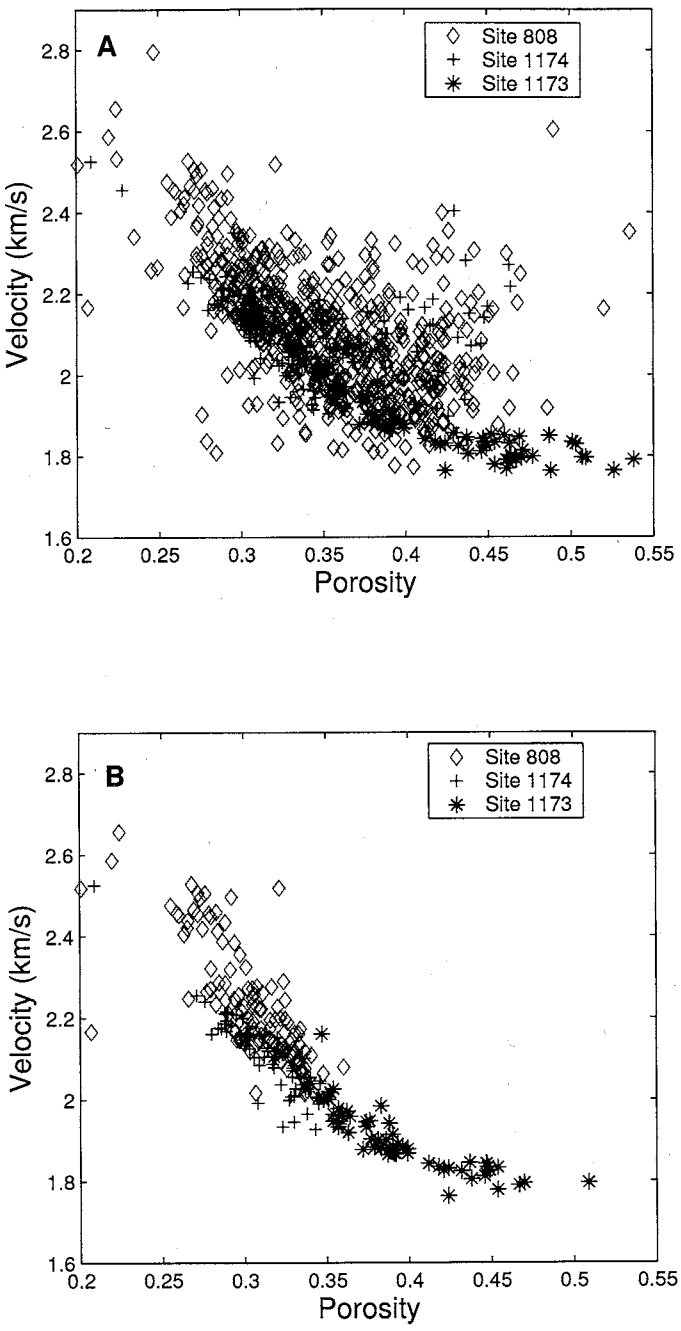

Figure 5.6: Velocity versus porosity for in-situ corrected core data for Sites 1173, 1174 and 808. A) Sediments above and below the décollement and B) Underthrust sediments (i.e below the décollement).

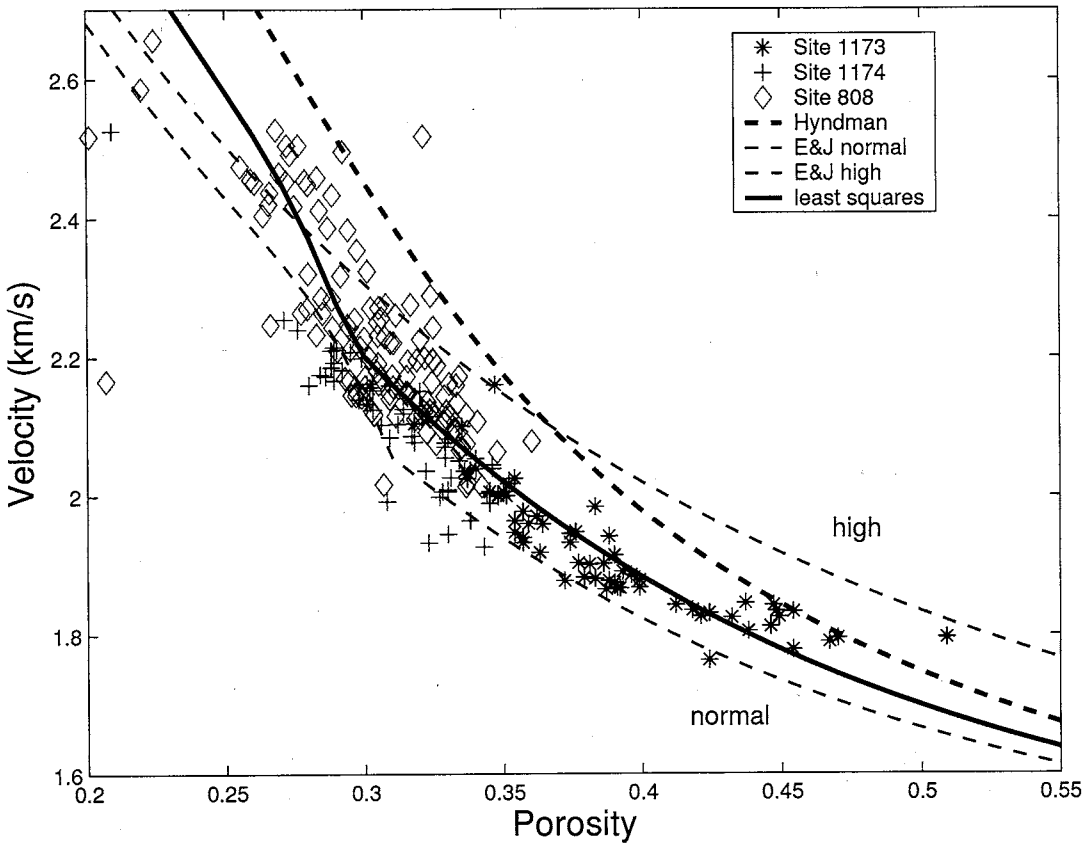

Figure 5.7: Empirical velocity-porosity formulations for the underthrust sediments for Site 1173, 1174 and 808. The least squares fit is plotted with a shale fraction of 1. The formulations for normal- and high-consolidation (Erickson and Jarrard, 1998) and plotted as well as the formulation from Hyndman et al. (1993).

parameter	fit	error (±)	error (%)	EJ normal	EJ high
A	0.746	0.379	51	0.739	1.11
B	0.532	0.327	61	0.552	0.178
C	0.124	0.171	137	0.130	0.135
v_{sh}	1.057	0.041	4	—	—
ϕ_c	0.295	0.006	2	0.31	0.39

Table 5.1: Parameters and the associated error for the nonlinear least-squares fit results and the corresponding parameters from the Erickson and Jarrard (1998) normal- and high-consolidation formulations.

In addition to the Erickson and Jarrard (1998) formulations, the velocity-porosity relationship from Hyndman et al. (1993) for Site 808 is plotted for comparison (Fig. 5.7): porosity (ϕ) is given in terms of compressional velocity (V in km/s)

$$\mathrm{P} = -1.180 + 8.607(1/\mathrm{V}) - 17.89(1/\mathrm{V})^2 + 13.94(1/\mathrm{V})^3 \qquad (5.5)$$

The ISONIC LWD velocity data from Sites 1173 (Fig. 4.1) and 808 (Fig. 4.3) are plotted (Fig. 5.8) to compare to the results obtained for the core measurements. The Site 1173 data are described accurately by the least squares fit and lie almost totally within the bounds of the Erickson and Jarrard (1998) formulations. The Site 808 data are extremely scattered and do not follow any apparent trend in velocity-porosity space.

The predicted velocities are compared to the measured velocities (Fig. 5.9). The parameters fit to the Shikoku Basin data accurately predict velocity for this particular data set. There is no trend towards either under- or over-predicting.

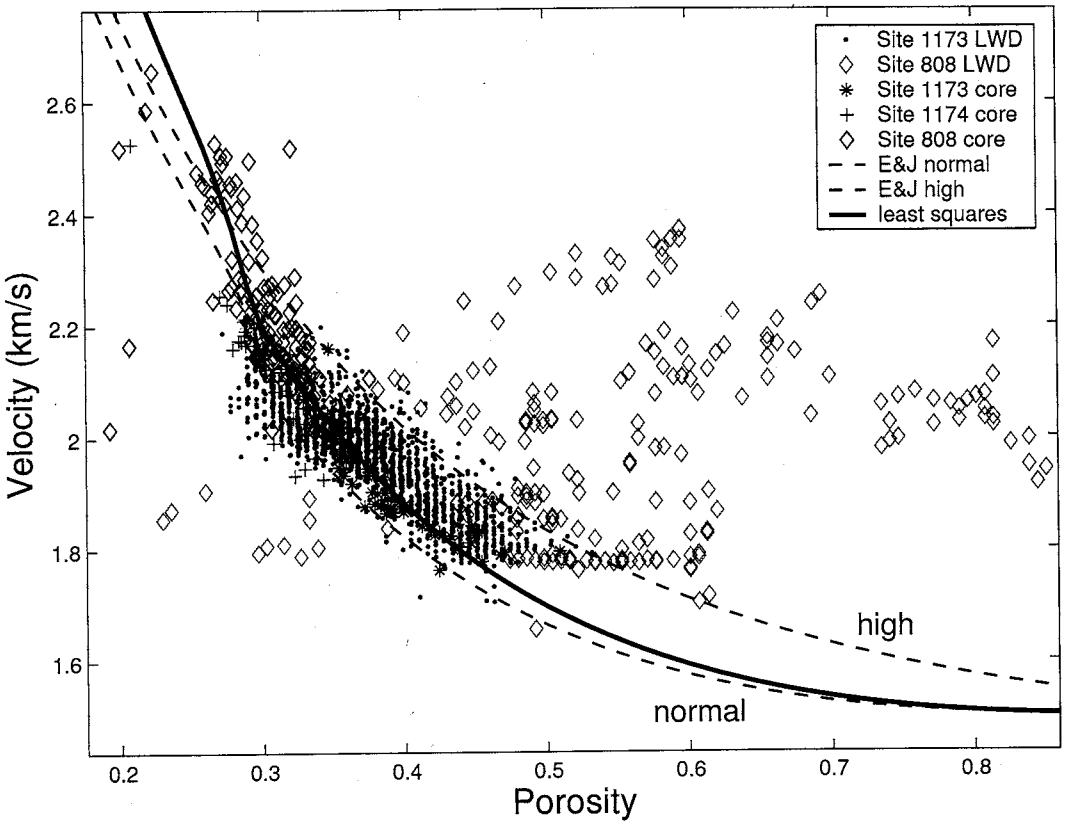

Figure 5.8: LWD ISONIC velocity data compared with the empirical velocity-porosity formulations for the underthrust sediments for Site 1173, 1174 and 808. The formulations for normal- and high-consolidation (Erickson and Jarrard, 1998).

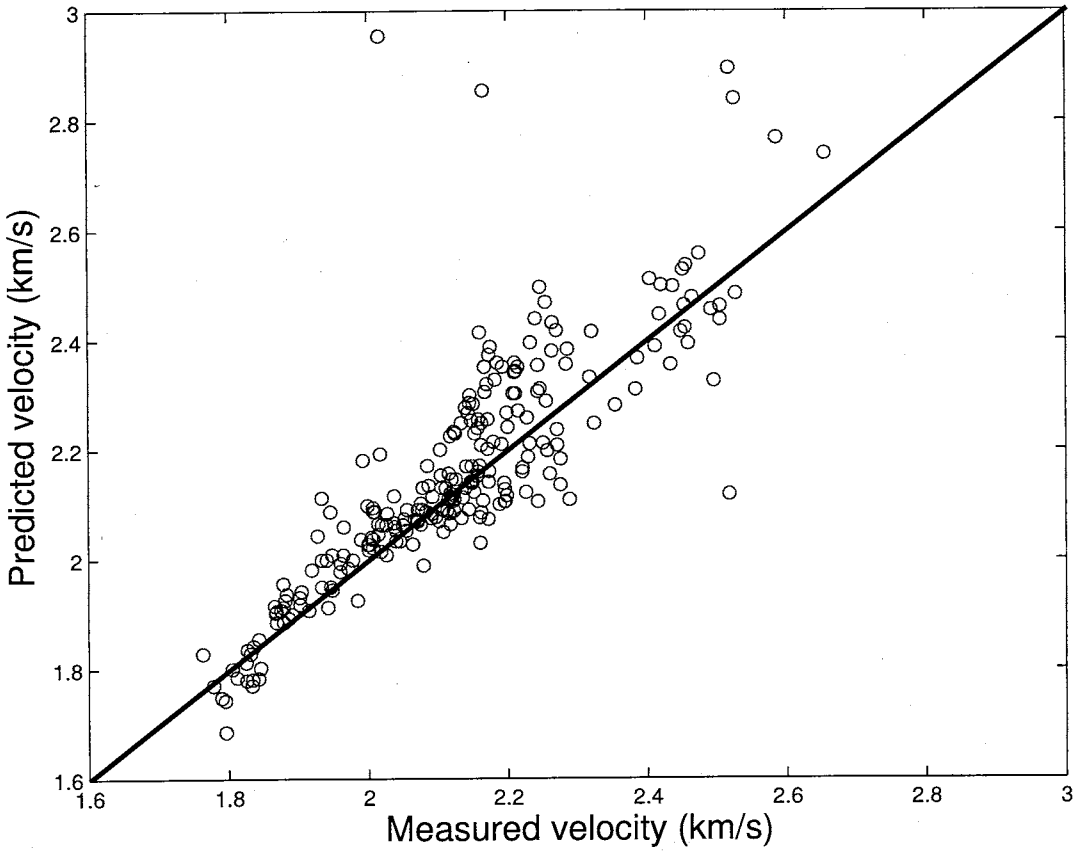

Figure 5.9: Predicted and measured velocities using the nonlinear least-squares parameter fitting results.

5.7 Discussion: Velocity-porosity Relationship

The velocity versus porosity plots for the sediments at Sites 1173, 1174 and 808 (Fig. 5.6A and B) clearly indicate that the sediments above and below the décollement exhibit different characteristics. This is illustrated by the absence of a trend in increasing velocity with decreasing porosity. This is most likely due both to a more varied lithology in the sediments above the décollement and to differing tectonic histories. When only the underthrust sediments are plotted (Fig. 5.6B) a clear trend of increasing velocity with decreasing porosity and a critical porosity transition are apparent. This is especially true for the Site 808 data and to a lesser extent, Site 1174. The underthrust sediments follow the normal-consolidation trend proposed by Erickson and Jarrard (1998) as is expected for underthrust sediments which have been subjected primarily to burial compaction stresses (Davis et al., 1983; Morgan and Karig, 1995).

The results of the parameter fitting for the underthrust sediments indicate that a critical porosity transition is crossed at $\sim$0.30. Whereas a single critical porosity value can be accurately fit to this data set, it appears that the critical porosity transition occurs over a range of porosities for Site 808. The median value of this range is $\sim$0.31 which agrees relatively well with the value obtained in the parameter fitting.

The parameter fitting provided a best-fit shale fraction value of $\sim$1.06. One possible explanation for an unphysical shale fraction being fit is the lack of lower porosity, higher velocity data to constrain this parameter. The average shale fraction of 0.32 calculated from the shale fraction log (Fig.5.5) suggests

that a lower value would more accurately describe these data. However, the shale fraction log for Site 1173 is probably not accurate due to the lack of representative sand and shale baselines. Further analysis needs to be done to accurately determine which shale fraction best describes the Shikoku Basin underthrust sediments.

It is also important to note that the values of the shale fraction significantly affects the values determined for the critical porosity in the parameter fitting. An improved fit could probably be obtained by holding the shale fraction constant (at a value representative of the sediments at Site 1173) and allowing the critical porosity to vary.

The relationship derived by Hyndman et al. (1993) does not appear to fit either the lower or higher porosity sediments as well as the formulations suggested by Erickson and Jarrard (1998). The Hyndman et al. formulation does follow roughly the same trend but systematically overestimates the velocity, especially for porosities near the critical porosity transition. However, this formulation was derived only for Site 808 data and different in-situ corrections have been applied to the current core data set, which accounts for most of the differences.

5.8 Conclusions: Velocity-porosity Relationship

The underthrust sediments for Sites 1173, 1174 and 808 follow the global velocity-porosity trends proposed by Erickson and Jarrard (1998). The formulation for normal-consolidation is a better fit to the data than the high-consolidation model, as is expected for undeformed underthrust sediments.

New parameters fit to the normal-consolidation model using a standard nonlinear least squares algorithm provides a single best-fit equation which can be used to convert between velocity and porosity with reasonable uncertainty. This formulation will be used to predict porosity from seismic interval velocity for the underthrust sediments. The new formulation better predicts velocity for the Shikoku Basin sediments than any of the previously determined relationships.

A critical porosity threshold appears to be crossed somewhere between Sites 1174 and 808 at $\sim$0.30. While a single critical porosity value can be reliably fit to the data, there are a range of porosities for which velocity exhibits a transition to a stronger dependence on porosity.

CHAPTER 6

SITE 1173 PHYSICAL PROPERTIES CHANGES

The physical properties of sediments are affected by a variety of factors which include sediment composition, diagenesis, and deformational history. The characteristics of downhole physical properties changes at Site 1173, most notably in porosity and velocity, in the upper and lower Shikoku Basin facies suggests other factors in addition to consolidation play an important role in affecting these properties.

In the upper Shikoku Basin facies (Fig. 3.1), porosity deviates significantly from the normal compaction trends for these types of sediments (e.g. Hamilton, 1976). Seismic velocity in this interval also deviates from the expected trend of velocity increasing with depth (e.g. Hamilton, 1978). At the boundary between the upper and lower Shikoku Basin facies (Fig. 3.1), porosity suddenly decreases while there is little change in seismic velocity. Porosity and velocity values below this boundary in the lower Shikoku Basic facies generally follow normal compaction trends.

Measurements of seismic velocity and porosity from the upper and lower Shikoku Basin sediments are used here to constrain the factors contributing to the high porosities between 102 mbsf and 320 mbsf and the abrupt physical properties changes which occur at the upper/lower Shikoku Basin facies boundary. The relationship between velocity and porosity is also used to con-

strain the possible effects of cementation in this interval. As silica diagenesis is thought to play a significant role in both of these intervals (Shipboard Scientific Party, 2001a), the analysis will focus on the changes in physical properties expected during the opal-A to opal-CT and opal-CT to quartz transitions. The implications for the existence of a critical porosity transition in the upper Shikoku Basin sediments will also be examined in terms of diagenetic and cementation effects. Evidence for other diagenetic processes in addition to silica diagenesis will also be presented.

6.1 Site 1173 - Physical Properties

The large scale physical properties of the sediments at Site 1173 were described in section 4.4. In the current section, the anomalous characteristics in velocity and porosity will be described in greater detail for the upper and lower Shikoku Basin facies, focusing on changes which may be a result of diagenetic processes.

6.1.1 Upper Shikoku Basin Facies

Porosity

In the outer trench-wedge facies (0-102 mbsf), core porosity values decrease from 72-70% to 56-66% by 102 mbsf (Fig. 6.1). The values are significantly scattered in this interval primarily due to variations in lithology (Shipboard Scientific Party, 2001b). In the upper Shikoku Basin facies, porosity actually increases slightly from ~60% at the top of the unit to ~68% at 320 mbsf. Beginning at 320 mbsf, porosity abruptly decreases to ~50% by the base of the unit at 344 mbsf.

Wireline porosity data is only available between 78-336 mbsf (Fig. 6.2) and is generally in agreement with the core data in this interval, though with less variability. Above 102 mbsf the log values are too scattered to provide an accurate idea of the porosity trend in this interval. Beginning at 102 mbsf, porosity increases from ~58% to an average value of 63% by the base of the log at 336 mbsf. There are sharp decreases at 264 mbsf (54%) and 323 mbsf (50%) which roughly correspond to similar decreases in the core porosities.

Velocity

In contrast to the sharp changes in porosity which occur in the upper Shikoku Basin facies, the changes in seismic velocity are more subtle (Fig. 6.1). Between 102 mbsf and 230 mbsf, core velocity remains constant at ~1600 m/s (in the x-,y-,and z-directions). At 230 mbsf, the values begin to smoothly increase to ~1750 m/s at the base of the unit.

Wireline shear and compressional velocities also show a similar trend in this interval (Fig. 6.2). Compressional velocities increase only slightly between 102-220 mbsf from ~1580 m/s to ~1650 m/s. In contrast, shear velocities remain roughly constant at ~300 m/s in the same interval. At 220 mbsf, both compressional and shear velocities begin to increase at greater rates to V_p ~1740 m/s and V_s ~450 m/s at 320 mbsf. Between 320 mbsf and the base of the unit at 344 mbsf, the changes become more complex. Both velocity logs exhibit slight decreases at 325 mbsf and then smoothly increase over the next 5 m. Below this depth (~330 mbsf), the values are significantly more scattered but a sharp drop begins at ~344 mbsf and continues to the base of each log at 363 mbsf.

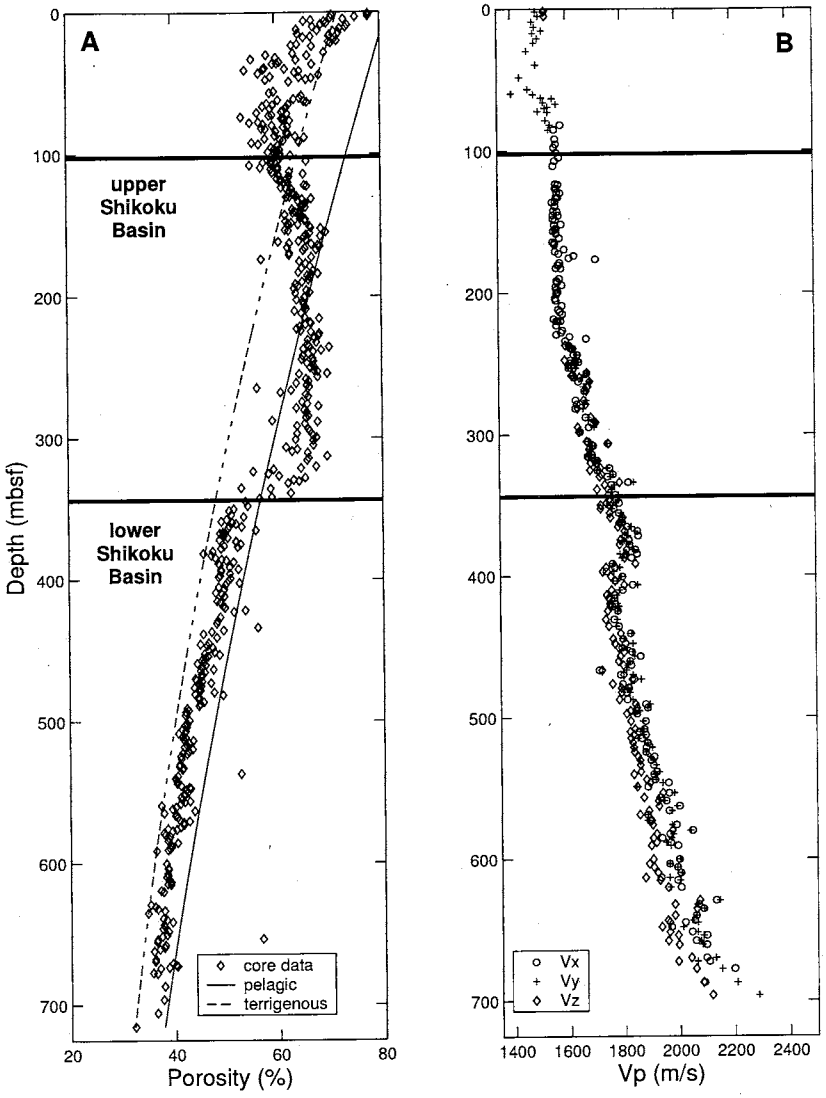

Figure 6.1: A) Core porosity data for Site 1173. The boundaries of the upper and lower Shikoku Basin facies are indicated by the black lines. The curves plotted are from Hamilton (1976) for pelagic clay (solid line) and terrigenous sediment (dashed line). B) Core velocity data for Site 1173. Velocity measurements are plotted for the x-, y-, and z- directions. The upper and lower Shikoku Basin facies are indicated by the black lines.

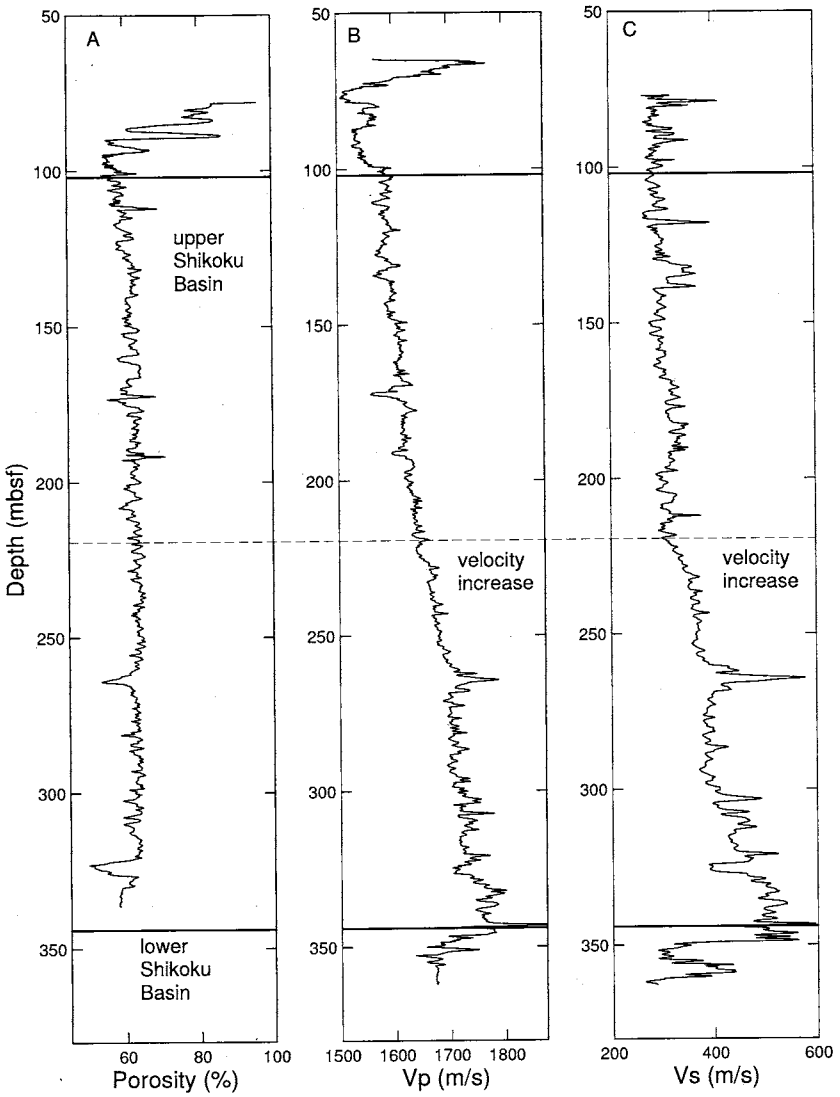

Figure 6.2: (A) Wireline porosity, (B) compressional-wave velocity, (C) and shear-wave velocity for Site 1173. The upper and lower Shikoku Basin boundaries are marked by the black line. The dashed line represent where changes in seismic velocity begin.

6.1.2 Lower Shikoku Basin Facies

In the lower Shikoku Basin facies, porosity generally follows the normal consolidation curve for fine-grained marine sediments (e.g. Hamilton, 1976; Fig. 6.1). At the top of the unit, porosity is ~50% and decreases smoothly to ~35% by the base of the unit at 688 mbsf. The values within this interval do not show as much scatter as in the upper Shikoku basin sediments which is most likely due to the more homogeneous nature of the sediments.

Core velocity measurements (Fig. 6.1) also generally increase within this unit from 1750 m/s at 344 mbsf to 2200 m/s at the base of the unit. There is a notable decrease at ~390 mbsf which corresponds to the approximate location of the projected décollement at this site.

6.2 Discussion: Site 1173 - Physical Properties

6.2.1 Silica Diagenesis

It has been suggested that processes associated with silica diagenesis affect the physical properties of the sediments in the upper and lower Shikoku Basin facies at Site 1173 (Shipboard Scientific Party, 2001b). The abnormal compaction trend in the upper Shikoku Basin facies and the abrupt changes in physical properties observed at the boundary between the upper and lower Shikoku Basin facies could be directly related to the solution and precipation of silica associated with one of the two silica phase transformations: opal-A to opal-CT and opal-CT to quartz.

The opal-A to opal-CT and opal-CT to quartz transitions both occur through a dissolution and reprecipitation mechanism (Hesse, 1988). Biogenic

silica (also called amorphous silica or opal-A) may not convert directly to quartz but instead go through an intermediate metastable phase. Because the solubility of opal-CT is intermediate between that of opal-A and quartz, opal-CT forms more easily from a solution in equilibrium with opal-A than does quartz (Isaacs et al., 1983). Eventually opal-CT is dissolved and reprecipitated as quartz.

Profiles of dissolved silicon with depth for pelagic sediments show a consistent increase with depth below the seafloor (Hesse, 1990). This gradual downward increase is often followed by an abrupt decrease which is consistent with reprecipitation of opal-A as opal-CT. A second maximum in the dissolved silicon profile may be observed at sufficient depth, which most likely corresponds to the dissolution of opal-CT and the reprecipitation as quartz.

6.2.2 Compaction Trend

In the upper Shikoku Basin facies, porosities are approximately 10-15% higher between 102-320 mbsf than the expected porosity for fine-grained marine sediments (e.g. Hamilton, 1976; Fig. 6.1). The sediments are best approximated by the curve for terrigenous sediments although the data lie roughly between the terrigenous curve and the pelagic clay curve (Hamilton, 1976). In contrast, seismic velocity remains approximately constant or increases only slightly over this interval. In order to clarify the relationship between velocity and porosity in this interval, a velocity-porosity crossplot is used. This type of plot can illustrate any trends present in the data and provide a means to compare with various theoretical (e.g. Nur et al., 1998; Dvorkin and Brevik, 1999) and empirical trends (e.g. Raymer at al., 1980; Erickson and Jarrard,

1998).

Core and wireline velocities (P- and S-wave) versus porosity are plotted in Figure 6.3. The data are broken down into the following depth intervals corresponding to the observed physical properties changes and facies boundaries: 78-102 mbsf, 102-220 mbsf, 220-320 mbsf, and 320-390 mbsf. The last interval crosses the boundary between the upper and lower Shikoku Basin facies and ends at what is interpreted as the beginning of the proto-décollement zone at Site 1173.

The sediments in the trench-wedge facies (78-102 mbsf) roughly follow the normal-consolidation trend of Erickson and Jarrard (1998) (Fig. 6.3A). With increasing depth, the upper Shikoku Basin sediments between 102-220 mbsf begin to exhibit an increase in compressional velocity while porosity remains relatively constant between 55% and 65% (Fig. 6.3A). This deviation is even more apparent between 220-320 mbsf as velocity continues to increase over an even smaller porosity range (60-65%). The sediments in the interval from 320-390 mbsf deviate from the overlying trends of increasing velocity and roughly follow the high-consolidation curve derived by Erickson and Jarrard (1998; Fig. 6.3A). The shear velocities (Fig. 6.3B) follow a similiar pattern to that of the compressional velocities. There is significantly more overlap between the values in different depth ranges, most notably around 220 mbsf. The similiar trends in the velocity-porosity plots would suggest that the same process is affecting both the compressional and shear velocities but does not cause as abrupt a response in the shear velocities.

The observed velocity-porosity trends suggest a critical porosity thresh-

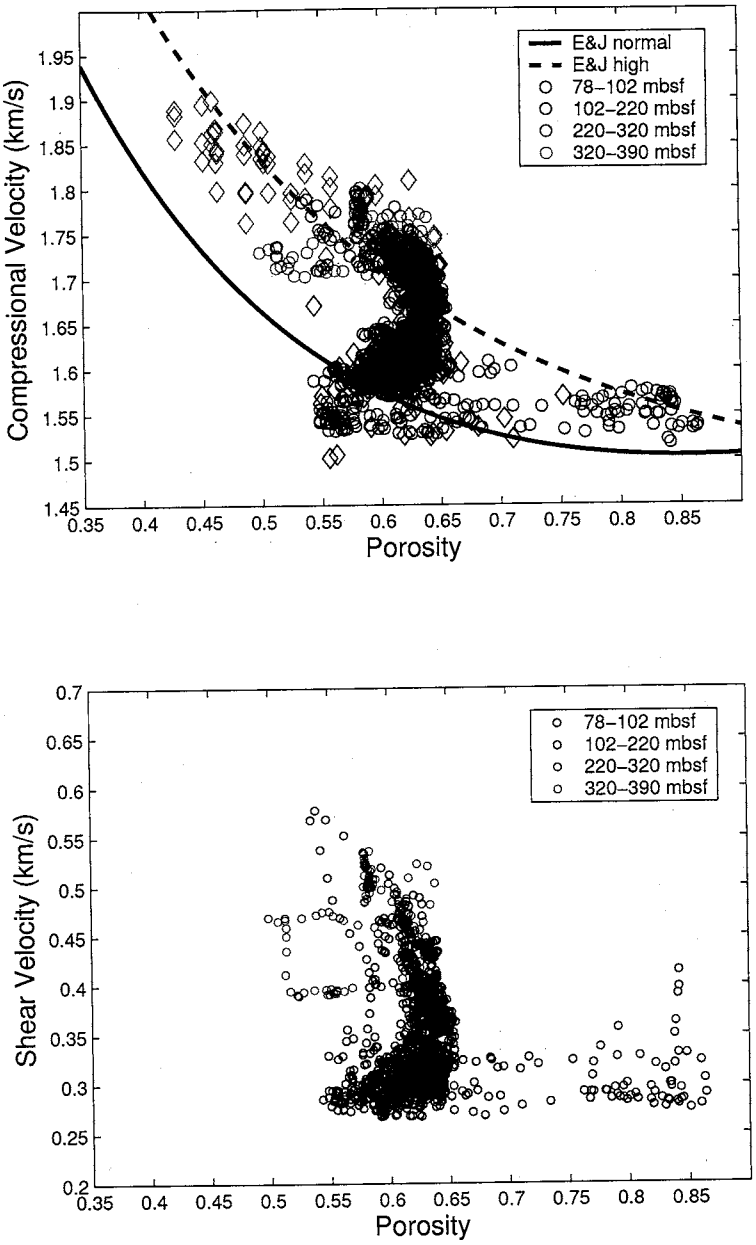

Figure 6.3: (A) Compressional velocity-porosity plot for core (diamonds) and wireline (circles) data for Site 1173. The different depth intervals are indicated by different colors. The thick black solid and dashed lines are for the normal- and high-consolidation curves derived by Erickson and Jarrard (1998). (B) Shear velocity-porosity plot wireline (circles) data for Site 1173. The depth intervals are the same as in (A).

old is crossed at ~65% (e.g. Nur at al., 1998). The critical porosity formulation (summarized in section 5.1) indicates that the sediments in the upper part of the upper Shikoku Basin facies are in a transition between a fluid-supported domain and a frame-supported domain. The existence of a critical porosity transition at such a high porosity in these sediments may indicate the presence of cementation effects which are contributing to the increased rigidity of the sediments between 220 mbsf and ~320 mbsf.

One possible cause for the observed compaction trend and cementation effects could be the precipitation of opal-A from the pore fluid and the deposition at the grain boundaries. The presence of this silica cement would serve to increase the rigidity of the sediments and prohibit a normal decrease in porosity. A plot of dissolved silicon (Fig. 6.4) for Site 1173 shows an increase in SiO_2 with depth which probably indicates the continued precipitation of opal-A from the pore fluid. An abrupt decrease in SiO_2 at ~344 mbsf most likely corresponds to the conversion of opal-A to opal-CT which results in a decrease of SiO_2 in the pore fluid. The breakdown of the opal-A cement is directly related to the processes observed at the upper/lower Shikoku Basin facies boundary.

6.2.3 Upper/Lower Shikoku Basin Facies Boundary

The boundary between the upper and lower Shikoku Basin facies is defined as the deepest occurrence of a fresh volcanic ash bed containing glass shards (Shipboard Scientific Party, 2001a). This boundary was chosen within a gradational change from ash to siliceous claystone which occurs over tens of meters. It has therefore been suggested that the upper/lower Shikoku Basin

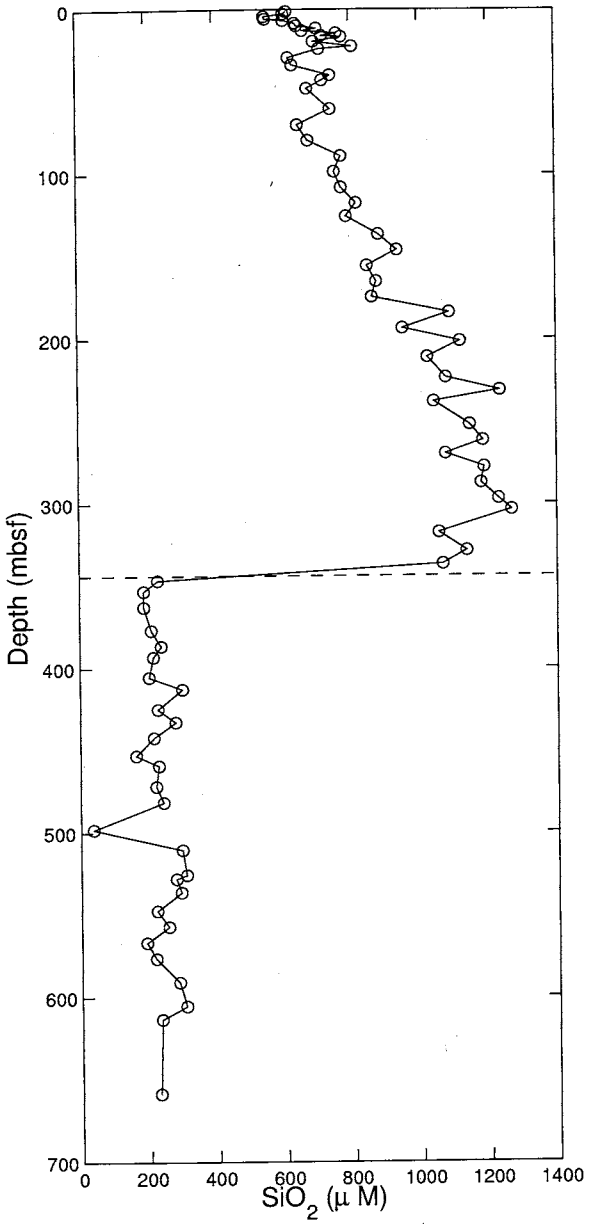

Figure 6.4: Profile of dissolved silicon (SiO_2) for Site 1173. The dotted line marks the boundary between the upper and lower Shikoku Basin facies at ~344 mbsf. Data from Shipboard Scientific Party (2002b).

facies boundary is largely diagenetically controlled (Shipboard Scientific Party, 2001a). This is supported by significant changes in sediment physical properties which have been observed across this boundary. The most notable change is an abrupt decrease in core porosity from ~60% to ~50% between ~320 and 344 mbsf. In addition, the amount of dissolved silicon (SiO_2) in the interstital fluid abruptly decreases at this boundary (Fig. 6.4). The combined decrease in porosity and dissolved silicon at this boundary could be directly related to the solution-precipation of silica.

The physical properties changes at the upper to lower Shikoku Basin facies boundary were originally interpreted as caused by the transition from opal-CT to quartz (Shipboard Scientific Party, 2001a). However, further analysis suggests the observed changes are instead caused by the transition from opal-A to opal-CT. This is supported by the observation of Nobes et al. (1992) for sediments in the Japan Sea that the opal-A/opal-CT boundary occurs at or near a lithologic boundary while the opal-CT/quartz transition often lies within a lithologic unit and is not as distinct as the first transition. In addition, the opal-A/opal-CT transition is often correlated with a significant seismic reflector (Nobes et al., 1992). A strong seismic reflector is observed at Site 1173 between 320-360 mbsf (Shipboard Scientific Party, 2002a) which correlates to the abrupt changes in porosity and density and is consistent with a high reflection coefficient.

In addition, the presence of opal-CT and zeolites in the lower Shikoku Basin siliceous claystones (Wilson et al., 2003) suggests they could be a product of the opal-A/opal-CT transition. Zeolites are natural byproducts of the opal-

A/opal-CT reaction in the presence of the clay minerals illite and smectite (Kastner, 1979, 1981) which are present in both the upper and lower Shikoku Basin sediments (Sunderland and Morgan, 2003).

Because seismic velocity is both directly and indirectly affected by porosity changes, the behavior of the compressional and shear velocities across the boundary should be also be affected. As porosity decreases as a result of enhanced compaction accompanying the dissolution of opal-A, the velocity should begin to increase. Nobes et al. (1992) observed velocities reaching maximum values just below the opal-A/opal-CT boundary and then decreasing. A similiar trend may be present in the wireline compressional and shear velocity logs at ~320 mbsf (Fig. 6.2). There is a noticeable increase at 320 mbsf followed by an immediate decrease, after which velocity begins to increase again.

6.2.4 Other effects

Cementation effects could also be caused by the existence of a fine smectite clay phase within the upper Shikoku Basin facies (Sunderland and Morgan, 2003). The decrease in porosity at the base of the upper Shikoku Basin facies (344 mbsf) may be due to smectite-illite diagenesis which causes a breakdown in the cement. However, the fine-grained phase is also observed in the lower Shikoku Basin facies which would argue that the smectite clay is not the sole cause of the abnormal compaction trend.

An additional possible explanation for the observed high porosities in the upper part of this unit is the presence of high pore fluid pressure prohibiting the normal compaction of the sediments. However, seismic velocities would not

then be expected to change in this interval, yet both compressional and shear velocities increase at 220 mbsf while porosity remains constant with depth. In addition, the existence of a critical porosity transition would not be consistent with high pore pressures and undercompaction.

6.3 Conclusions: Site 1173-Physical Properties

An analysis of Shikoku Basin sediment physical properties indicates that silica diagenesis plays an important role in affecting the properties of these sediments. Silica diagenesis is the most likely cause of 1) the abnormal compaction trend in the upper Shikoku Basin facies and 2) the abrupt physical properties changes associated with the upper and lower Shikoku Basin facies boundary.

The upper Shikoku Basin sediments exhibit abnormally high porosities as a result of early cementation which is later destroyed. The most likely cementing phase is the precipitation of opal-A onto grain boundaries. This accounts for both the high porosities and the increases in seismic velocity observed between 220-320 mbsf. Evidence for a critical porosity transition at $\sim$65% further strengthens the argument for cementation. The similar trends observed in the velocity-porosity crossplots for both compressional and shear velocities suggest that both are affected by the same process.

The boundary between the upper and lower Shikoku Basin facies appears to be largely controlled by further silica diagenesis. The opal-A to opal-CT transition causes the abrupt decrease in porosity observed between 320-344 mbsf. The effects of this transition on seismic velocity are more subtle but are

observed in both the compressional and shear wireline velocities in addition to seismic reflection data. Detailed sedimentological characterization could provide evidence to confirm or refute this hypothesis in the future.

APPENDIX A

LABORATORY MEASUREMENTS

Laboratory measurements of P-wave velocity, S-wave velocity, and porosity were conducted under elevated pressure on whole-round core samples from Site 1173. The purpose of these tests was to study the dynamic elastic properties of the sediments in the context of stress paths in the accretionary prism (e.g. Karig and Morgan, 1994). Ultrasonic velocities of the samples were measured under effective pressures between 0.25 and 32 MPa.

A.1 Methods

Site 1173 samples were obtained from whole-round cores obtained during drilling on ODP Leg 190. Cylindrical sub-samples were cut manually to an average diameter of 19.5 mm with lengths ranging between 25.3 and 30.8 mm. The cylindrical sub-samples were then jacketed and inserted into the pressure vessel apparatus. The pressure vessel used to measure ultrasonic velocities is described in greater detail by Gettemy (2001). Ultrasonic waves are generated using a PZT-crystal in the endplates on either end of the sample. A standard pulse transmission method (Christensen, 1985) is used to determine the velocities. The digitally recorded waves are used to determine the arrival times of the P- and S- phases. For the 1173 samples, only the P-wave arrival time has been identified as further processing is necessary to determine the

S-wave arrival times.

The length of the sample during testing was measured using a linear potentiometer transducer (LPT). Using the initial porosities of the samples and the length changes during testing under elevates pressure, the porosity at each pressure step was determined. The velocity in each sample is then determined by dividing the length of the sample by the travel time through the sample. The P-wave velocities and porosities under elevated pressure for each sample are plotted in Figure A.1.

A.2 In-situ values for velocity and porosity

Using the laboratory measurements, velocity and porosity for in-situ conditions were determined by calculating the effective pressure for each sample depth. This was done using the LWD density log for Site 1173 and assuming hydrostatic pore pressure. The effective pressure for each sample depth location is plotted in Figure A.1.

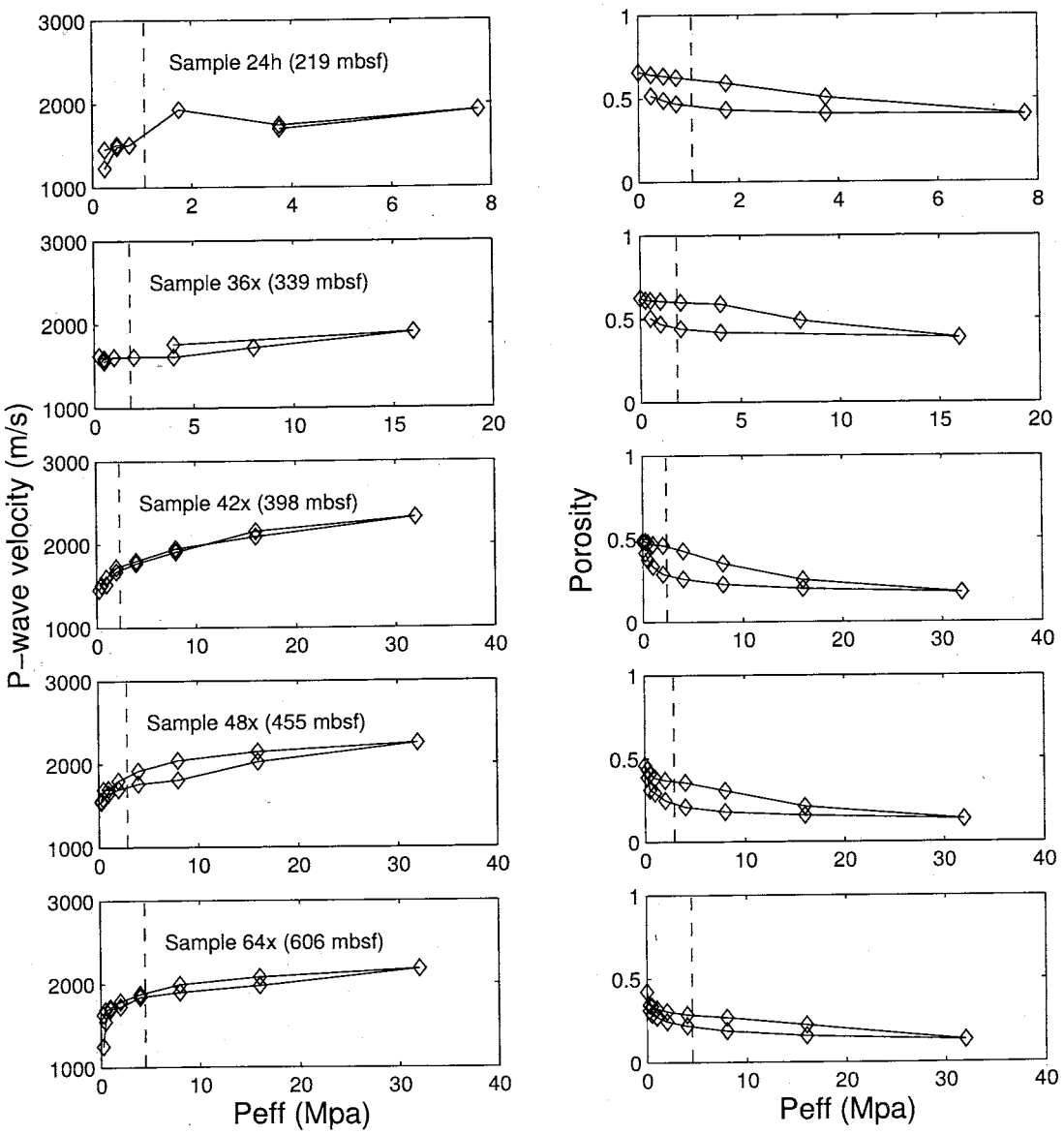

Figure A.1: Laboratory measurements of P-wave velocity and porosity for Site 1173 samples.

REFERENCES

Bangs, N.L., Taira, A., Kuramoto, S., Shipley, T.H., Moore, G.F., Mochizuki, K., Gulick, S.S., Zhao, Z., Nakamura, Y., Park, J.-O., Taylor, B.L., Morita, S., Ito, S., Hills, D.J., Leslie, S.C., Alex, C.M., McCutcheon, A.J., Ike, T., Yagi, H., and Toyama, G., 1999. U.S.-Japan Collaborative 3-D seismic investigation of the Nankai Trough plate-boundary interface and shallow most seismogenic zone. *Eos*, 80:F569.

Blangy, J.P., Strandeness, S., Moos, D., Nur, A., 1993. Ultrasonic velocities in sands-revisited. *Geophysics*, 58:344-356.

Boyce, R.E., 1976. Definitions and laboratory techniques of compressional sound velocity parameters and wet-water content, wet-bulk density, and porosity parameters by gravimetric and gamma-ray attenuation techniques. In Schlanger, S.O., Jackson, E.D., et al., *Init. Repts. DSDP*, 33: Washington (U.S. Govt. Printing Office), 931-958.

Byrne, T., and Fisher, D., 1990. Evidence for a weak and overpressured décollement beneath sediment-dominated accretionary prisms. *J. Geophys. Res.*,95:9081-9097.

Chamot-Rooke, N., Renard, V., and Le Pichon, X., 1987. Magnetic anomalies in the Shikoku Basin: a new interpretation. *Earth Planet. Sci. Lett.*, 83:214-228.

Christensen, N.I., 1985, Measurements of dynamic properties of rock at elevated temperatures and pressures. *In* Pincus, H.J., and Hoskins, E.R. (Eds.), *Measurement of Rock Properties at Elevated Pressures and Temperatures, ASTM STP 869*, American Society for Testing and Materials, Philadelphia, 93-107.

Davis, D., Suppe, J., and Dahlen, F.A., 1983. Mechanics of fold-and-thrust belts and accretionary wedges. *J. Geophys. Res.*,88:1153-1172.

Dresser Atlas, 1982. Well Logging and Interpretation Techniques, The Course for Home Study, 3rd ed., Dresser Atlas Ind.

Dvorkin, J., and Brevik, I., 1999. Diagnosing high-porosity sandstones: strength and permeability from porosity and velocity. *Geophysics*, 64: 795-799.

Erickson, S., and Jarrard, R., 1998. Velocity-porosity relationships for water-saturated siliciclastic sediments. *J. Geophys. Res.*,103:30385-30406.

Goldberg, D., 2003a. Data report: Reprocessing of wireline sonic logs in turbidites and hemipelagic sediments at ODP Site 1173. *In* Mikada, H., Moore, G.F., Taira, A., Becker, K., Moore, J.C., and Klaus, A. (Eds.), *Proc. ODP, Sci. Results*, 190/196 [Online]. Available from World Wide Web: http://www-odp.tamu.edu/publications/190196SR/209/209.htm. [Cited 2003-12-01]

Hamilton, E.L., 1965. Sound speed and related properties of sediments from Experimental Mohole (Guadulupe Site). *Geophysics*,30:257-261.

Hamilton, E.L., 1976. Variations of density and porosity with depth in deep-sea sediments. *J. Sediment. Petrol.*, 46:280-300.

Hamilton, E.L., 1978. Sound velocity gradients in marine sediments. *J. Acoust. Soc. Am.*, 64:909-922.

Han, D., Nur, A., Morgan, D., 1986. Effects of porosity and clay content on wave velocities in sandstones. *Geophysics*, 51:2093-2107.

Hesse, R., 1988. Origin of chert: diagenesis of biogenic siliceous sediments. *Geosci. Can.*, 15:171-192.

Hills, D.J., Moore, G.F., Bangs, N.L., and Gulick, S.S., and Leg 196 Shipboard Scientific Party, 2001. Preliminary results from integration of 2D PSDM and ODP Leg 196 velocity data in the Nankai accretionary prism. *Eos. Trans. Am. Geophys. Union*, 82:F1221.

Hyndman, R.D., Moore, G.F., and Moran, K., 1993. Velocity, porosity, and pore-fluid loss from the Nankai subduction zone accretionary prism. *In* Hill, I.A., Taira, A., Firth, J.V., et al., *Proc. ODP, Sci. Results*, 131: College Station, TX (Ocean Drilling Program), 211-220.

Isaacs, C.M., Pisciotto, K.A., and Garrison, R.R., 1983. Facies and diagenesis of the Monterey Formation, California: a summary. *In* Iijima, A., Hein, J.R., and Siever, R. (Eds.), *Siliceous Deposits in the Pacific Region*: Amsterdam (Elsevier), 247-282.

Jarrard, R.D., Dadey, K.A., Busch, W.H., 1989. Velocity and density of sediments of Erik Ridge, Labrador Sea: COntrol by porosity and mineralogy. *Proc. ODP, Sci. Results*, 105: College Station, TX (Ocean Drilling Program), 811-835.

Kano, K., Kato, H., Yanagisawa, Y., and Yoshida, F., 1991. Stratigraphy and geologic history of the Cenozoic of Japan. Geol. Surv. Jpn., 274:114.

Karig, D.E., and Angevine, C,L., 1986. Geologic constraints on subduction rates in the Nankai Trough, *In* Kagami, H., Karig, D.E., and Coulbourn, W.T., et al., *Init. Repts. DSDP*, 87: Washington (U.S. Govt. Printing Office), 789-796.

Karig, D., and Morgan, J., 1994. Tectonic deformation: stress paths and strain histories. *In* Maltman A., (Ed.) *The Geological Deformation of Sediments*: Chapman and Hall, 167-204.

Kastner, M., 1979. Zeoloites. *In* Burns, R.G. (Ed.), *Marine Minerals. Rev.* Mineral., 6:111-122.

Kastner, M., 1981. Authigenic silicates in deep-sea sediments: formation and diagenesis. *In* Emiliani, C. (Ed.), *The Sea*, 7: New York (Wiley Interscience), 915-980.

Kobayashi, K., and Nakada, M., 1978. Magnetic anomalies and tectonic evolution of the Shikoku inter-arc basin. *J. Phys. Earth*, 26:391-402.

Lallemant, S., Byrne, T., Maltman, A.J., Karig, D.E., and Henry, P., 1993. Stress tensors at the toe of the Nankai accretonary prism: an application of inverse methods to slickenlined faults. *In* Hill, I.A., Taira, A., Firth, J.V., et al., *Proc. ODP Sci. Results*, 131: College Station, TX (Ocean Drilling Program), 103-122.

Le Pichon, X., Henry, P., and Lallemant, S., 1993. Accretion and erosion is subduction zones: The role of fluids, *Annu. Rev. Earth Planet. Sci., 21*, 307-331.

Moore, G.F., Taira, A., Bangs, N.L., Kuramoto, S., Shipley, T.H., Alex, C.M., Gulick, S.S., Hills, D.J., Ike, T., Ito, S., Leslie, S.C., McCutcheon, A.J., Mochizuki, K., Morita, S., Nakamura, Y., Park, J.O., Taylor, B.L., Toyama, G., Yagi, H., and Zhao, Z., 2001. Data report: Structural setting of the Leg

190 Muroto transect. *In* Moore, G.F., Taira, A., Klaus, A., et al., *Proc. ODP, Init. Repts.*, 190, 1-14 [CD-ROM]. Available from: Ocean Drilling Program, College Station TX.

Moore, G.F., Taira, A., Kuramoto, S., Shipley, T.H., and Bangs, N.L., 1999. Structural setting of the 1999 U.S.-Japan Nankai Trough 3-D seismic reflection survey. *Eos*, 80:F569.

Moore, G.F., Taira, A., Klaus, A., et al., 2001. New Insights into deformation and fluid flow processes in the Nankai Trough accretionary prism: Results of Ocean Drilling Program Leg 190. *Geochemistry, Geophysics, Geosystems* [Online]. Available from the World Wide Wed: http://www.agu.org/journals/gc/.

Moore, J.C., 1989. Tectonics and hydrogeology of accretionary prisms: role of the décollement zone. *J. Struct. Geol.*, 11:95-106.

Morgan, J.K., and Karig, D.E., 1995. Décollement processes at the Nankai accretionary margin, Southeast Japan: Propagation, deformation, and dewatering. *J. Geophys. Res.*, 100:15221-15231.

Nobes, D.C., Murray, R.W., Kuramoto, H., Pisciotto, K.A., and Holler, P., 1992. Impact of silica diagenesis on physical properties variations, *In* Pisciotto, K.A., Ingle, J.C., von Breymann, M.T., Barron, J. et al., (Eds.). *Proc. ODP Sci. Results*, 127/128: College Station, TX (Ocean Drilling Program), 3-31.

Nur, A., Mavko, G., Dvorkin, J., Galmudi, D., 1998. Critical porosity: A key to relating physical properties to porosity in rocks. Leading Edge, 17:357-362.

Raymer, L.L., Hunt, E.R., Gardner, J.S., 1980. An improved sonic transit time-to-porosity transform. *Trans. SPWLA Annu. Logging Symp.*, 21st:P1-P13.

Schlumberger, 1989. Log Interpretation Principles/Applications: Houston (Schlumberger Educ. Services), SMP-7017.

Schlumberger, 1995. DSI-Dipole Sonic Imager: Houston (Schlumberger Wireline and Testing), SMP-5128.

Seno, T., The instantaneous rotation vector of the Philippine Sea Plate relative to the Eurasian Plate, *Tectonophysics, 42*, 209-226, 1977.

Seno, T., Stein, S., and Gripp, A.E., A model for the motion of the Philippine Sea plate consistent with NUVEL-1 and geological data, *J. Geophys. Res., 98*, 17941-17948, 1993.

Shipboard Scientific Party, 1991a. Geological background and objectives. *In* Taira, A., Hill, I.A., Firth, J.V., et al., *Proc. ODP, Init. Repts.*, 131: College Station, TX (Ocean Drilling Program), 5-14.

—, 1991b. Site 808. *In* Taira, A., Hill, I.A., Firth, J.V., et al., *Proc. ODP, Init. Repts.*, 131: College Station, TX (Ocean Drilling Program), 71-269.

Shipboard Scientific Party, 2001a. Leg 190 summary. *In* Moore, G.F., Taira, A., Klaus, A., et al., *Proc. ODP, Init. Repts.*, [CD-ROM], 190: College Station, TX (Ocean Drilling Program), 1-87.

—, 2001b. Site 1173. *In* Moore, G.F., Taira, A., Klaus, A., et al., *Proc. ODP, Init. Repts.*, [CD-ROM], 190: College Station, TX (Ocean Drilling Program), 1-147.

—, 2001c. Site 1174. *In* Moore, G.F., Taira, A., Klaus, A., et al., *Proc. ODP, Init. Repts.*, [CD-ROM], 190: College Station, TX (Ocean Drilling Program), 1-149.

—, 2001d. Explanatory Notes. *In* Moore, G.F., Taira, A., Klaus, A., et al., *Proc. ODP, Init. Repts.*, [CD-ROM], 190: College Station, TX (Ocean Drilling Program), 1-51.

Shipboard Scientific Party, 2002a. Leg 196 summary: deformation and fluid flow processes in the Nankai Trough accretionary prism: logging while drilling and Advanced CORKs. *In* Mikada, H., Becker, K., Moore, J.C., Klaus, A., et al., *Proc. ODP, Init. Repts.*, 196: College Station TX (Ocean Drilling Program), 1-29.

—, 2002b. Site 1173. *In* Mikada, H., Becker, K., Moore, J.C., Klaus, A., et al., *Proc. ODP, Init. Repts.*, 196: College Station TX (Ocean Drilling Program), 1-97.

—, 2002c. Site 808. *In* Mikada, H., Becker, K., Moore, J.C., Klaus, A., et al., *Proc. ODP, Init. Repts.*, 196: College Station TX (Ocean Drilling Program), 1-68.

—, 2002d. Explanatory Notes. *In* Mikada, H., Becker, K., Moore, J.C., Klaus, A., et al., *Proc. ODP, Init. Repts.*, 196: College Station TX (Ocean Drilling Program), 1-53.

Sunderland, E.B., and Morgan, J.K., 2003. Microstructural variations in sediments from the toe of the Nankai accretionary prism: results of scanning electron microscope analysis. *In* Mikada, H., Moore, G.F., Taira, A., Becker, K., Moore, J.C., and Klaus, A. (Eds.), *Proc. ODP, Sci. Results*, 190/196 [Online].*in press*

Taira, A., J. Katto, M. Tashiro, M. Okamura, and K. Kodama. The Shimanto Belt in Shikoku, Japan-evolution of Cretaceous to Miocene accretionary prism. *Mod. Geol.*,12:5-46, 1988.

Taira, A., and Niitsuma, N., Turbidite sedimentation in the Nankai Trough as interpreted from magnetic fabric, grain size, and detrital modal analyses, *In* Kagami, H., Karig, D.E., and Coulbourn, W.T., et al., *Init. Repts. DSDP*, 87: Washington (U.S. Govt. Printing Office), 611-632, 1986.

Taira, A., Tokuyama, H., and Soh, W. Accretion tectonics and evolution of Japan. *In* Ben-Avraham, Z. (Ed.), *The Evolution of Pacific Ocean Margins*: Oxford Univ. Press, 100-123, 1989.

Wilson, M.E.J., Hirano, S., Fergusson, C.L., Steurer, J., and Underwood, M.E., 2003. Data report: Sedimentological and petrographic characteristics of volcanic ashes and siliceous claystones (altered ashes) from Sites 1173, 1174, and 1177, Leg 190. *In* Mikada, H., Moore, G.F., Taira, A., Becker, K., Moore, J.C., and Klaus, A. (Eds.), *Proc. ODP, Sci. Results*, 190/196 [Online]. Available from World Wide Web: http://www-odp.tamu.edu/publications/190196SR/204/204.htm. [Cited 2003-12-01]

Wyllie, M.R.J., Gregory, A.R., Gardner, G.H.F., 1956. An experimental investigation of factors affecting elastic wave velocities in heterogeneous and porous media. *Geophysics*, 21:41-70.

Yoneshima, S., Endo, T., Pistre, V., Thompson, J., Campanac, P., Mikada, H., Moore, J.C., Ienaga, M., Saito, S., and Leg 196 Scientific Party, 2003. Processing leaky-compressional mode from LWD sonic data in shallow ocean sediments: ODP sites in Nankai Trough, *Proc. 6th Ann. SEGJ Int'l Sympos.*, Japan.

This thesis is accepted on behalf of the
Faculty of the Institute by the following committee:

Advisor

1-20-04
Date

I release this document to the New Mexico Institute of Mining and Technology.

Student's Signature

1-20-04
Date